Denise E. Kirschner
Stewart T. Chang
Thomas W. Riggs
Nicolas Perry
Jennifer J. Linderman

Toward a multiscale model of antigen presentation in immunity

Authors' addresses
Denise E. Kirschner[1,2,4], *Stewart T. Chang*[1,4], *Thomas W. Riggs*[1], *Nicolas Perry*[1], *Jennifer J. Linderman*[2,3]
[1]Department of Microbiology and Immunology, University of Michigan Medical School, Ann Arbor, MI, USA.
[2]Department of Biomedical Engineering, University of Michigan, Ann Arbor, MI, USA.
[3]Department of Chemical Engineering, University of Michigan, Ann Arbor, MI, USA.
[4]Center for Computational Medicine and Biology, University of Michigan, Ann Arbor, MI, USA.

Correspondence to:
Denise E. Kirschner
Department of Microbiology and Immunology
University of Michigan Medical School
6730 Medical Science Building II
Ann Arbor, MI 48109, USA
Tel.: +1 734 647 7722
Fax: +1 734 647 7723
E-mail: kirschne@umich.edu

Acknowledgements
This work was supported under grant numbers HL68526, HL72682, and LM00902701. The authors thank Simeone Marino and Seema Bajaria for use of results from their published work.

Immunological Reviews 2007
Vol. 216: 93–118

Immunological Reviews
0105-2896

Summary: A functioning immune system and the process of antigen presentation in particular encompass events that occur at multiple length and time scales. Despite a wealth of information in the biological literature regarding each of these scales, no single representation synthesizing this information into a model of the overall immune response as it depends on antigen presentation is available. In this article, we outline an approach for integrating information over relevant biological and temporal scales to generate such a representation for major histocompatibility complex class II-mediated antigen presentation. In addition, we begin to address how such models can be used to answer questions about mechanisms of infection and new strategies for treatment and vaccines.

Keywords: *antigen presentation, mathematical models, multiscale, immunity, antigen-presenting cells*

Introduction

Biological systems are often explored in the laboratory at a reductionist scale. The idea is that if we understand everything at particular scales (most recently focused at the molecular scale), we will then understand the system as a whole; immunology is no exception. Of concern, however, is that the immune system spans multiple length (gene through body) and time (subsecond through lifetime) scales and that the immune response will likely only be completely understood through knowledge of how processes at these different scales work together. Such an integrative picture of a system is the desired outcome of multiscale modeling. In total, approaches that capture multiscale or system-wide features fall under the umbrella of systems biology.

Systems biology encourages a non-reductionist approach to model development, beginning with the simplest possible model. Coined 'reconstructionism' by M. Savageau (1), the idea is that biological systems are more than the sum of their parts and that integrative behavior occurs in a non-predictable fashion. The modeling process itself brings about an understanding of the underlying system, as components are captured

with mathematics and/or statistics. A minimal model is constructed and then grows in complexity, driven by new hypotheses that may not have been apparent from the phenomenological descriptions. With recent advances in information technology – fast and inexpensive computing power, global networking infrastructure, and comprehensive databases – modeling and simulation are becoming increasingly important biological tools. For the most part, these efforts have focused at a single scale, e.g. genomic/proteomic, cellular, tissue, organ, organ system, and whole body. Only now is there an emphasis to develop tools, techniques, algorithms, and mathematical theory to integrate seamlessly the continuum from the micro- to the macroscale. Multiscale modeling deals with spanning scales as diverse as from molecular to population. It can affect our understanding of biological processes and also further our predictive capabilities in biology. Multiscale algorithms are built and validated against experimentally derived data and observations.

The need for multiscale approaches in biology is recognized in the cardiovascular field, where a number of groups are developing methods to integrate molecular and cellular events with organ function (2, 3). In addition, multiscale approaches are now being considered for neural systems (4–6), tumor growth (7), the vasculature (8), and developmental biology (9). Multiscale approaches are also being applied in various engineering problems, for example in polymer science (10) and tissue engineering (11). We argue that immunology is also ripe for such a multiscale approach.

We focus in this article on antigen presentation through the major histocompatibility complex (MHC) class II pathway and its role in the immune response. We first review the relevant biological events and discuss the multiscale aspects of the process. We then present models that have been developed to address biological events occurring at various scales and give examples of applications to the study of disease dynamics. Finally, we discuss ways to begin to integrate models across scales.

The biology of antigen presentation

Antigen presentation is the process by which peptide fragments from the proteins of pathogens or the host are partially degraded and then displayed (or 'presented') on the surfaces of cells in complex with MHC molecules. Once bound to MHC, antigens can be recognized by cognate T cells, which then respond either by killing the original antigen-presenting cell (APC) or else by activating it along with other cells. While antigen presentation may appear to occur only at molecular and cellular scales, events at other scales also affect the outcome. For instance, antigen presentation to naive T cells occurs within the larger context of the lymph node (LN), and other chemical signals (e.g. cytokines produced by other cells) within the LN or the topology of the LN itself may affect whether APCs are able to contact and activate T cells. Similarly, the ability of effector T cells to traffic out of the LN and throughout the body will affect the time course of an infection. The success of antigen presentation therefore depends on events occurring at multiple biological scales (*Fig. 1*).

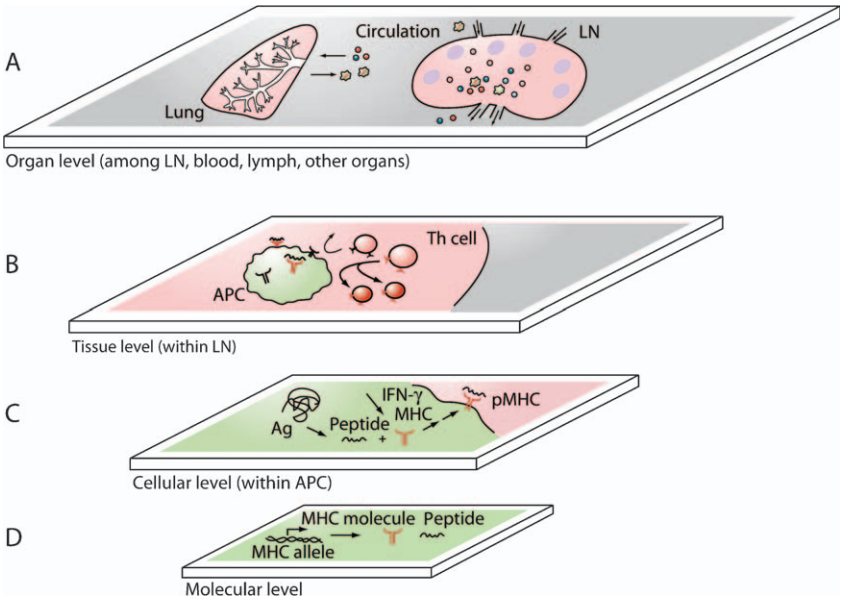

Fig. 1. Key events in antigen presentation. Biological scales are represented here as physical levels. (A) Multicompartmental system of blood, lymphatics, and particular organs/sites of interest. (B) LN environment wherein APCs interact with T cells. (C) Intracellular pathways leading to pMHC complexes on the surface of an APC. (D) Molecular level interactions between peptide and MHC are influenced by genetic differences among MHC II alleles. Ag, antigen.

Peptide–MHC binding

A key event in antigen presentation is the binding of peptide to one of two classes of MHC molecule. All nucleated human cells perform antigen presentation to some extent by expressing MHC I molecules that sample peptides from the cytoplasm. However, some cells are also capable of presenting peptides derived from exogenous antigens using MHC class II molecules; these specialized cells are known as professional APCs. In this review, we focus on macrophages and dendritic cells (DCs), although B cells can also serve as APCs. [A recently discovered pathway for presenting lipid antigens, the CD1 pathway, will not be considered here; reviewed by De Libero and Mori (12)].

For the most part, the two classes of MHC molecule sample different sources of antigen and take divergent pathways through the cell. Proteins found in the cytoplasm, including those produced by viruses, are degraded (or 'processed') into shorter peptides by the main protein turnover machinery of the cell, the proteasome. A subset of these peptides is transported into the endoplasmic reticulum (ER) by the transporter associated with antigen processing (TAP). Binding between peptides of a particular length (8–10 amino acids) and MHC class I molecules then occurs within the ER, and the resulting complexes are trafficked to the cell surface. In contrast, antigens from pathogens that do not reside in the cytoplasm, including bacteria and parasites, are generally first taken up by the cell and then processed in the endosomal pathway. Cathepsin proteases located within the endosomal pathway become activated by the increasingly acidified environment and cleave the protein antigens into peptides of shorter lengths. Binding between extracellular-derived peptides of varying lengths (often greater than nine amino acids) and MHC class II molecules then occurs later in this pathway or in a specialized vacuole that branches off known as the MHC class II-binding compartment. Peptide–MHC II (pMHC II) complexes are then trafficked to the cell surface, as in the case of the class I pathway. In both cases, the final stage is recognition of the complexes by cognate T-cell receptors (TCRs), either on the surface of $CD8^+$ cytotoxic T cells (in the case of MHC I) or on the surface of $CD4^+$ helper T cells (in the case of MHC II).

One theme that arises from this cursory overview of both antigen presentation pathways is the importance of high-affinity binding. Peptides that bind a particular MHC molecule weakly – or alternatively MHC variants that bind a particular peptide weakly – are expected to lead to relatively few pMHC complexes on the APC surface. Binding affinities of pMHC complexes can be measured *in vitro* using a number of different techniques. In the most common assay, a competitive binding assay, various concentrations of the peptide of interest are used to displace the binding of a labeled reporter peptide. The concentration at which 50% of the reporter peptide is displaced is equal to the IC_{50}, which approximates the equilibrium dissociation constant of a pMHC complex, K_D. More precisely, IC_{50} is related to K_D according to the following formula:

$$K_D = IC_{50}\left(1 + \frac{L_r}{K_r}\right)^{-1}$$

where L_r and K_r represent the concentration of the reporter peptide and the equilibrium dissociation constant of the reporter pMHC complex, respectively (13). These parameters frequently vary by protocol, L_r explicitly so and K_r by virtue of being specific to each combination of peptide and MHC (14–16). Alternatively, K_D values and even association and dissociation rate constants can be determined by other techniques including radiolabeling and fluorescence polarization methods (17). Several online databases including MHCPEP (18), MHCBN (19), and AntiJen (20) now store pMHC binding affinities. These databases currently contain measurements on approximately 13 000, 14 000, and 24 000 peptides, respectively. In the former two databases, IC_{50} values are not available directly but can be inferred from the four-tiered classification used by both databases: high affinity indicates IC_{50} of <1 nM; moderate, IC_{50} of 1–100 nM; low, IC_{50} of 100 nM–10 μM; and no binding, IC_{50} of >10 μM. An IC_{50} of 500 nM is also commonly used as a threshold to differentiate binding from non-binding (21). In AntiJen, IC_{50} is reported directly whenever possible.

The greater significance of binding affinity to antigen presentation can also be discerned from the epidemiological literature. Various MHC alleles have been correlated with increased susceptibility to diseases, particularly chronic diseases of an autoimmune or an infectious nature (22). Examples of diseases associated with particular MHC alleles include type I diabetes, rheumatoid arthritis, malaria, and tuberculosis. Because most polymorphisms in MHC molecules occur within the peptide-binding region, it is reasonable to assume that binding to either peptide or TCR is affected. The detailed mechanisms behind these associations have not yet been elucidated, although several hypotheses exist (22–24). Furthermore, a correlation between pMHC affinity and magnitude of the immune response at the cellular level has been shown (25, 26). We provide a full treatment of this topic elsewhere (Chang *et al.*, manuscript in preparation).

Cellular processes controlling display of pMHC complexes

pMHC binding is by no means the only step that is regulated in the antigen presentation pathway. Other steps are controlled

dynamically, e.g. by cell-to-cell contact or the constantly changing cytokine environment surrounding the APC, and allow antigen presentation to be fine-tuned. We describe these steps and others relevant to the MHC II-mediated pathway in more detail below (*Fig.* 2) (reviewed in 27).

Antigens for the MHC II-mediated pathway are generally internalized by one of three routes before converging on the endosomal pathway: phagocytosis, fluid-phase pinocytosis, and receptor-mediated endocytosis. Internalized antigens then progress through increasingly acidified endosomes and are exposed to low pH-activated cathepsins that degrade the antigens into smaller peptides (28). These peptides then either bind MHC II molecules or are directed to lysosomes for degradation.

MHC II expression normally occurs at low levels in resident APCs but can be upregulated or downregulated by the cytokine environment. Interferon-γ (IFN-γ) is one cytokine that affects MHC II expression. After IFN-γ binds to its receptor on the APC surface, a signal is propagated through the Janus kinase (JAK) signal transducer and activator of transcription (STAT) pathway that increases the level of class II transactivator (CIITA) in the cell. CIITA acts as the master regulator of MHC II transcription, and increased levels of CIITA lead to parallel increases in MHC II expression several hours after exposure to IFN-γ. Nascent MHC II molecules enter the ER and are coupled to another protein, invariant chain (Ii). The luminal domain of Ii binds the peptide-binding groove of MHC II, protecting it from proteases, while the cytoplasmic domain of Ii directs the two molecules to the endosomal pathway. After reaching the endosomal pathway, MHC II molecules retain a remnant of Ii, the class II invariant peptides (or CLIP), until released by the enzyme H2-/human leukocyte antigen (HLA)-DM (29). Here, antigenic peptides compete for binding to MHC II with self-peptides that are present at high levels and may bind more than 80% of the available MHC II in the absence of exogenous peptides (30, 31). In complex with either self-peptides or exogenous peptides, MHC II molecules then traffic to the cell surface, where they may remain stable for days until recognized by $CD4^+$ T cells or are internalized and degraded.

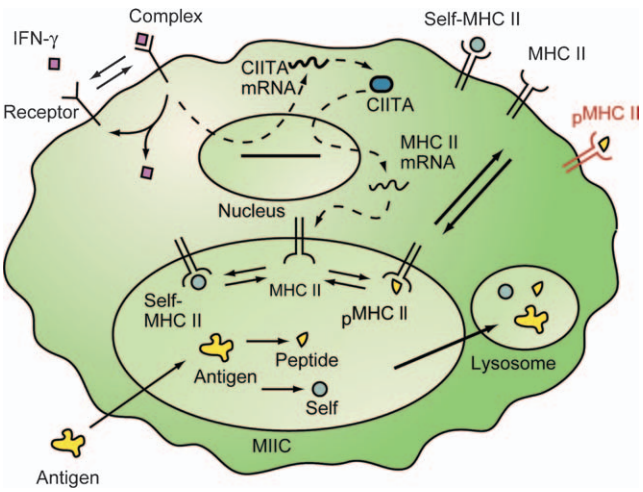

***Fig.* 2. Molecular and intracellular events influencing the display of pMHC II complexes on a single APC.** One-step reactions are indicated by solid arrows, while regulatory processes (which may involve several reactions) are indicated by dashed arrows.

Macrophages and DCs express not only MHC II molecules but also costimulatory and adhesion molecules necessary to engage T cells. Both macrophages and DCs derive from a common precursor, the monocyte, which differentiates into one of the two cell types based on environmental cues (32, 33) [B cells, another APC type and not a focus of this review, are derived from hematopoietic cells in the bone marrow (27)]. Macrophages and DCs are found in overlapping distributions within the body in areas such as the LNs, and there is even evidence to suggest these cells can re-differentiate from one class to the other (34).

Differences between macrophages and DCs occur in the rates at which they perform processes related to antigen presentation. DCs express 10–100 times the number of MHC II molecules expressed by macrophages and also perform antigen uptake at generally increased rates (35, 36). Consistent with these findings, fewer DCs are required to activate T cells than macrophages (35). More importantly, these cells play different roles in the overall development of the immune response. DCs take up antigen at the site of infection and migrate to LNs to present antigen, while macrophages primarily perform their function as APCs at the infection site (37).

Cellular interactions in the context of the LN

Once on the surface of the APC, pMHC II complexes can elicit partial or full activation of T cells, depending at least in part on the number of peptides presented and the number of TCR engaged (i.e. bound to pMHC). Relatively few measurements of pMHC–TCR affinity have been made, although some are available in AntiJen (20). A single pMHC on the APC surface has been shown to be sufficient to elicit an intracellular release of calcium within the T cell, while full activation is generally acknowledged to require hundreds of complexes as gauged by the release of interleukin (IL)-2, a cytokine that initiates localized T-cell division (also known as clonal expansion) (38, 39). In addition, there is evidence that a quantitative relationship exists between surface pMHC levels and the magnitude of T-cell response, assuming pMHC levels exceed a lower threshold (38, 40–42). The effects of antigen presentation

therefore may be sensitive to variations in a number of contributing intracellular processes.

During the course of an infection, antigen presentation occurs at two major sites. First, within the LN, antigen presentation events that are responsible for initiating an adaptive immune response occur and are driven mainly by DCs. Second, at the site of infection, macrophages participate in antigen presentation events that sustain immune responses. The tissue-level context strongly influences the dynamics of antigen presentation and recognition. For example, the LN environment restricts cytokines and chemokines to a microenvironment, allowing efficient signaling to occur.

As the early events of immunity likely determine the success of the response, understanding events within the LN is a critical first step. There are approximately 700 LNs, each roughly 1–5 cm^3 in size, distributed throughout the human body, and those closest to a given site of infection will be engaged in infection dynamics. Some infections are systemic, involving not a particular tissue site but instead the blood or multiple epithelial sites; in these cases, many different LNs will be involved at some level.

LNs are connected through a series of lymphatics that serve as the highway between the LNs, entering into each LN through afferent lymph ducts and leaving through the medullary sinuses that flow into a single efferent lymph duct (*Fig.* 3). Blood vessels also feed into the lymphatic system, both directly into the LNs at high endothelial venules (HEVs) and at junctures throughout. Lymphatics then return cells to blood through a common conduit: the thoracic duct (43). APCs circulate into LNs through the afferent lymphatics, while T cells enter through the HEVs (44, 45). Once in the LN, $CD4^+$ T cells sample the surface of APCs for pMHC complexes within the LN paracortex (T cell region of LN).

When a $CD4^+$ T cell encounters an APC and its TCR binds its cognate pMHC on the surface of the APC, a series of events follows leading to T-cell activation. At the interface between APC and T cell, pMHC, TCR, and costimulatory and adhesion molecules aggregate into a structure known as the immunological synapse (IS) (46). Recently, the IS has been the subject of intense investigation, and several theories exist as to how this intricate structure forms and functions (47). If recognition occurs, T cells become activated and begin secreting IL-2. These T cells differentiate and become fully activated in response to further environmental cues and additional cell–cell interactions with APCs (48, 49). Experimentally, these changes can be tracked by measuring the amount of radioactive-labeled nucleotides incorporated by T cells as they divide. The ability to quantify T-cell activation in turn provides an assay for antigen presentation (50). In one commonly used *in vitro* assay, cultured APCs are pulsed with a particular model antigen (e.g. ovalbumin) and then exposed to T-cell hybridoma cells specific for that antigen.

The composition of individual LNs can be determined by extracting the LNs from animals (pre- and post-infection) and analyzing them by flow cytometric methods, such as fluorescence-activated cell sorting (51–54). From these studies, it is clear that immune cell numbers increase dramatically during an immune response. However, what cannot be ascertained from these studies are the spatial dynamics that occur within an LN and are known to play a role in the success of antigen presentation events.

With the advent of two-photon intravital microscopy, a technique that allows visualization of cells within a tissue environment, it is becoming increasingly clear that T-cell responses in LNs *in vivo* are much different form what has been observed *in vitro* because of environmental factors as well as the inherent structure of the LN (55–57) (*Fig.* 3). Using intravital techniques, one can observe T cells and DCs interacting as they travel through the paracortoid region of the LN. T cells display rapid motion in LNs, moving at an average of 10–12 μm/min and a peak velocity of 25 μm/min. On the smallest time scale, the motion varies linearly with time, having a mean free path ≈30 μm and changing path direction on average every 3 min (57). Over longer time scales (up to 20 min), displacement-squared varies almost linearly versus time, characteristic of a random walk and quantified by the motility coefficient ≈65 μm^2/min (58). Because T cells must traverse a LN in <48 h, as observed in classical studies of lymph circulation (59), their motion must be biased toward migration from entry at the afferent lymph to exit at the efferent lymph over the time scale of hours to days. If the motion through the entire LN conformed to a random walk with a motility coefficient of 65 μm^2/min, T-cell migration through the LN would take 24 h to move 600 μm from the starting point and more than 10 days, on average, to be displaced 2 mm. Both of these distances would represent unrealistically slow movement through the entire LN, particularly because the T-cell motility decreases when bound to a DC or when the T cell enters the medullary sinuses on the path to exit from the LN through the efferent lymphatic. (Note these calculations do not refer to the total path length but rather the net displacement from the starting point for a completely random walk.) Alternatively, these observations could be reconciled by invoking a random walk in the paracortical region of the lymph node and a biased, non-random walk into and out of that region. The microanatomy of the LN consists of a fibroblastic reticular cell network that can aid in directing

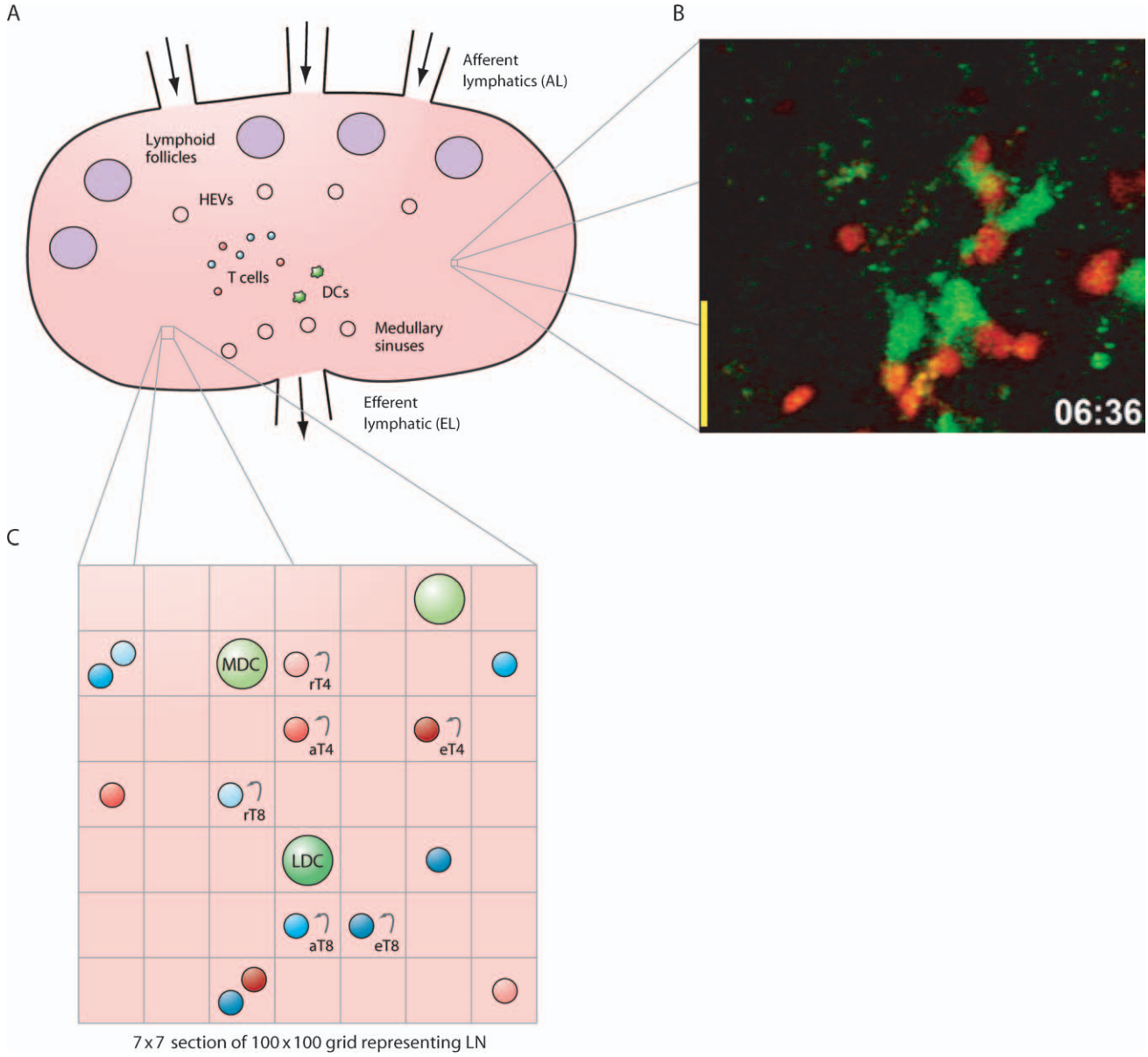

***Fig. 3.* APCs and T cells interacting in the LN.** (A) Schematic of the LN. Afferent lymphatics empty into an LN, bringing APCs such as DCs that rarely leave the LN after arrival. T cells enter from the blood through the HEVs and exit through the efferent lymphatic. Dynamic interactions between APCs and T cells occur within the LN. (B) Intravital microscopy image showing the interaction of DCs (green) with T cells (red) within a section of the LN measuring 75 μm by 100 μm. Image from Miller *et al.* (63), with courtesy of *J Exp Med* and Mark Miller. (C) Lattice representation of an LN. A 7 × 7 grid is shown, where each unit space is the size of one DC, the largest cell type of those included in our simulations. T4, $CD4^+$ T cell; T8, $CD8^+$ T cell; r, resting; a, activated; e, effector; M, mature; L, licensed.

naïve T cell motion from the HEV to the paracortical areas (60). Furthermore, there is evidence in support of chemokine mediated attraction to the B follicles within the LN and to dendritic cells (61, 62). The extent to which random vs. directed motion contribute to optimal scanning of T cells by DCs for a rare cognate match has not been completely resolved. For a full treatment of this topic see (Riggs, T, Walts, A, Perry, P, Lynch, J, Linderman, J, Miller, M and Kirschner D. in preparation). Once a T cell binds to a DC with cognate antigen, its movement slows with binding lasting over a period of 10–15 h; clusters of T cells form around the DC, followed by swarming behavior of the T cells (63). Following this prolonged contact, both T cells and DC are activated [a fully activated DC is known as a licensed DC (LDC)] and T-cell proliferation begins (63).

To date, the processes captured by intravital microscopy technique represent very short time scales (minutes to hours) and occur over very small length scales (100 μm). Intravital

microscopy therefore captures a relatively small region of an entire LN, which can be larger than 1 cm^3 (and during infection grows even larger) and over a relatively brief time slice of an adaptive immune response that occurs over days to weeks. Further, simultaneous assessment of the processes occurring at different biological scales and time scales cannot be made by microscopy studies at this point. Image analysis is also time-consuming and complicated (55). As a result, many details regarding human LNs and the role these structures play in determining the outcome of the immune response remain to be elucidated (43).

The anatomy of the LN is important in discerning not only antigen presentation events but also requirements for trafficking into and out of the node. The structure and composition of HEVs determine T-cell entry into the LN (43, 64). During inflammation, cells that would normally exit from the LN might be blocked (65), leading to a sudden increase in cell numbers within the LN. While T cells enter through HEVs, DCs enter through the afferent lymphatics. After entry, DCs position themselves around HEVs (66, 67), allowing for efficient scanning by T cells immediately upon entry. Thus, the dynamic processes of trafficking into and out of the LN can greatly enhance the opportunity for antigen presentation to occur as well as determine its success (68).

Circulation of immune cells between blood and other physiological compartments

Ultimately, the success of the initiated immune response also depends on the ability of APCs to traffic to LNs and the ability of activated T cells to return to the site of infection, events dependent on input from multiple compartments including both the blood and the lymphatic systems. Of the more than 10^{11} naive T cells in constant circulation between the blood and the lymphatics, only a small proportion (10%) of non-naive T cells travel to the LNs on a regular basis. The other 90% circulate to the spleen, lung, liver, bone marrow, and other parts of the lymphatic system (69, 70). The purpose of this trafficking is to maintain immune surveillance in all parts of the body, so as to rapidly mobilize cells to sites of antigen challenge (71). For example, to understand the dynamics of infection with *Mycobacterium tuberculosis* (*Mtb*), one would need to consider the flow of immune cells between the LN and the lung (72, 73). The entire process of T-cell trafficking through LNs occurs over a 24–48 h time frame, with T cells spending the majority of their time in the lymphatics (74, 75). This circulation is critical for driving LN dynamics.

Trafficking of DCs from the site of infection where they encounter and take up antigen to the closest draining LN is the first step post-infection in the cascade of events leading to adaptive immunity. DCs must migrate from peripheral sites into the paracortical regions of the LNs to optimally encounter T cells (68). During the course of migrating from the site of infection to the LN, DCs undergo a number of changes collectively referred to as maturation. These changes include a cessation of the rapid pinocytic rates DCs display at peripheral sites and an increase in MHC class II expression. Upon reaching the LN, DCs carrying antigen are classified as mature (MDC). Although data support the presence of immature DCs in the LN, it is unclear how they come to be there. Immature DCs either must migrate in or are generated from monocyte precursors in the LN. Naive T cells are constantly circulating through the lymphatic system to encounter antigen presented on DCs. The adhesion molecule L-selectin (CD62L), expressed on naive $CD4^+$ T cells, is essential for entry of cells into the LN (76). The process of T cells circulating to the LNs in this fashion is referred to as homing (76). Effector T cells that have been primed in the LN must circulate back to the site of infection to participate in the clearance of the pathogen.

Pathogens regularly interfere with antigen presentation

Pathogens regularly interfere with immune processes (77). Because pathogens meet APCs continually as a first line of defense, it should not be surprising that viral and bacterial pathogens have evolved ways to inhibit multiple aspects of antigen presentation both directly and indirectly. Cytomegalovirus is a viral pathogen that has been shown to inhibit antigen presentation by interrupting the MHC II expression pathway (78). Recently, both Ebola and Hanta viruses have also been shown to interfere with antigen presentation (79).

An example of a bacterial pathogen that inhibits antigen presentation is *Mtb*. *Mtb* is the number one cause of death due to infectious disease in the world today (2 billion people infected). Upon entering the lungs, *Mtb* is taken up by resident macrophages or DCs, adapts to the intraphagosomal environment, and either becomes dormant or slowly replicates (80). *Mtb* is known to inhibit antigen presentation in chronically infected macrophages. The mechanisms by which *Mtb* achieves this inhibition have not been completely elucidated, although several hypotheses have been proposed (81–83). Mathematical modeling is a tool that can be used to explore the mechanisms by which pathogens inhibit antigen presentation.

Approximately 14 million people have died of the acquired immunodeficiency syndrome (AIDS) pandemic. Over 40 million people are estimated to be human immunodeficiency virus (HIV) positive, with about 4.9 million newly infected per year (84). Despite the impressive amount of research on HIV

pathogenicity and immunology, there is no effective vaccine or cure. Ultimately, our capacity to fully treat or immunize against HIV is limited by our incomplete knowledge of the mechanisms behind the immune response to HIV-1, the more prevalent and virulent type of the virus. Because HIV-1 uses the CD4 receptor on the surface of both T cells and macrophages for entry and infection, these important immune cells are greatly affected. Specifically, the numbers and functionality of these important immune cell classes diminish during infection, eventually leading to AIDS. Although HIV-1 is not known to directly inhibit MHC II presentation, it disrupts many of the important events that occur both upstream and downstream of T-cell recognition of pMHC complexes. A comprehensive model of antigen presentation encompassing adaptive immunity would allow for a greater understanding of how the immune response fails in HIV-1 and highlight targets for therapeutic intervention.

Antigen presentation as a multiscale process

Processes at several length and time scales govern antigen presentation and the development of an immune response (*Table 1 panel A*). The binding affinity of MHC II and peptide depends not only on the peptide sequence but also on the particular MHC II allele. pMHC binding is a molecular-scale event that is embedded in the context of single-cell-scale events, e.g. antigen uptake, MHC synthesis, antigen processing, and pMHC trafficking and display, which occur on a time scale of minutes to hours. In the LN environment, a tissue space of ≈ 1 cm^3, T cells meet APCs, and over a period of hours to days cells interact with APCs, divide, migrate through the LN, and exit. Finally, at the organ/organism scale, exiting cells go to sites of infection to participate in the adaptive immune response, which bears a length scale that encompasses the entire organism and a time scale of days to weeks.

***Table 1*. Relevant scales and features associated with the different antigen presentation events**

A. Scale			B. Modeling	
Biological	Time	Length	Dynamics	Model type
Molecular	10^{-2}–10^{2} s	10^{-9}–10^{-8} m	Deterministic, continuous	Statistical
Cellular	10^{1}–10^{3} s	10^{-5} m	Deterministic, continuous	Mathematical: ODE
Tissue	10^{4}–10^{5} s	10^{-3}–10^{-2} m	Stochastic, discrete	Algorithmic: ABM
Organ/ organism	10^{5}–10^{6} s	10^{-2}–1 m	Deterministic	Hybrid: ODE + ABM

A, biological events occur at different time and length scales and B, modeling approaches described here.

Of primary interest is the entire multiscale system: the immune response and the outcome of infection in a host. How this complex system depends on various parameters and even therapeutic manipulations at the different scales is a key goal. Yet given its complexity, the entire multiscale system is presently impossible to study in an experimental setting. Thus, we turn instead to building a multiscale model of antigen presentation and its role in the immune response.

Certainly, there has been a wealth of basic science performed at the various biological scales attempting to elucidate these processes. Indeed, events at each scale of the antigen presentation process are likely to affect the overall development of the immune response. Models built to elaborate the relevant interactions and dynamics at each of the individual scales are the first step toward understanding a larger picture. Ultimately, the integration of such models will provide a multiscale model of the process.

Such a multiscale approach will allow us to address questions that bridge biological scales. For example, can particular MHC alleles (molecular scale) give rise to more pMHCs on the APC cell surface (cellular scale)? Can higher pMHC affinity (molecular scale) compensate for poorer APC uptake ability (cellular scale) or fewer APC or fewer highly specific T cells (tissue scale)? Could reduced display of pMHC by an APC (cellular scale) be compensated for by a longer residence time in the LN (tissue scale)? Will slowed cell circulation through the LN (tissue scale) slow or diminish the magnitude of the overall response (organ/organism scale)?

At the scale of an entire organism, a multiscale model can address issues related to infection sites and other organ involvement. For example, how large must variations in the affinities of peptides for MHC (molecular scale) be in order to significantly impact the response (organism scale), and can such variation in affinities offer a basis for disease association? Multiscale models are essential to show features that cannot be predicted by a focus on a single spatial or time scale. To begin to address these issues, we now present efforts made using modeling approaches at each of the scales and discuss how we might link these individual models to generate a multiscale model of antigen presentation.

Modeling approaches

Models at individual scales

It would be difficult to imagine a single experiment that could shed information on all the different spatial and time scales involved in antigen presentation. Similarly, constructing and validating a model encompassing all these events present

unique challenges. The approach we describe below is to build models at each of the different scales and then develop methods to link them together. For each of the biological scales represented in *Fig. 1*, different statistical, mathematical, or algorithmic models have been developed (*Table 1 panel B*).

At each scale, a decision needs to be made regarding the appropriate type of model to construct. Statistical models can be used for uncovering trends when large data sets are available. Here, an understanding of mechanisms is not necessary; rather, mechanisms may be inferred from the results of the analysis. Mathematical models involve equations to describe biological events, and these may be solved analytically or numerically. Algorithmic models are implemented on the computer as a detailed sequence of rules. Hybrid models are also possible. Several excellent texts are available that describe the use of each of these models in biology, particularly mathematical models (85–91). A limited number of texts are also available describing the biological applications of statistical models (92–94) as well as algorithmic models (89, 95).

Models may be categorized in one of several ways. First, models may be continuous or discrete. Continuous models treat entities not as individuals but as an averaged population or concentration, e.g. the concentration of a cytokine might vary continuously from 1 to 5 nM within an LN. Discrete models treat entities as individuals, e.g. a single cell could be tracked as it moves through an LN. Second, models may be stochastic or deterministic. Stochastic models have random events that affect the outcome, e.g. a cell may move to the right or to the left with equal probability. Each individual simulation will give a slightly different result. The results of multiple simulations can be averaged and standard errors obtained. Deterministic models, in contrast, yield the same result each time they are solved or simulated, capturing for example an average behavior of a molecular or cell population rather than particular outcomes.

Ultimately, the choice of modeling approach depends on considerations of the biological scale of interest – its spatial and time scales, the questions to be posed, whether tracking individual entities is important, etc.—as well as practical considerations such as available computing resources. In some cases, new insights may be found by using multiple approaches to a single problem (96).

Parameter estimation and sensitivity analysis

A critical issue to all models at any spatial or time scale is that of estimating parameter values (e.g. rate constants, concentrations, probabilities of a particular event, etc.). There are several approaches possible for estimating parameter values: (i) direct experimental determination of a parameter; (ii) simultaneous estimation of several parameters at once by fitting experimental data to a model (97); and (iii) estimation of a parameter based on known values for similar systems. In all cases, there is necessarily some uncertainty in the parameter value (for example, because of experimental error, differences in animal models, and technical limitations in kinetic measurements), and this leads to uncertainty in the output of any model using that parameter.

Because our models include parameters describing a large number of known biological processes, it is critical to understand the role that each of these parameters plays in determining output. Sensitivity analysis involves the correlation of variances in parameter values to variances in model output and is particularly useful when parameter values are not known with certainty. If simulations can be performed relatively quickly, all parameters can be varied simultaneously to ascertain those that contribute to significant variations in output variables. In the Latin hypercube sampling (LHS) algorithm, each parameter is assigned a distribution, typically uniform or normal and centered on a baseline or estimated value, allowing the effect of under- and overestimation to be examined. The entire range of each distribution is then sampled to generate a set of values for each parameter, and parameter values for each simulation are chosen to cover the entire parameter space in as few simulations as possible. Although originally applied for differential equation models (98, 99), we have recently adapted the algorithm for use in other types of models (100, 101). The extent to which each parameter affects the output can be quantified by one of several metrics including the partial rank correlation coefficient (PRCC). PRCC, like the more familiar Pearson correlation coefficient, varies between -1 and 1, indicating strongly negative and positive associations, respectively. A PRCC of 0 indicates no association. PRCC values can also be calculated at different time points of the simulation, allowing the relative importance of a particular parameter in determining model output to be tracked over time. In addition, a confidence interval can be determined for each PRCC, and differences between PRCCs can be tested for statistical significance (102). This test allows parameters to be ranked in order of effect they have on output by PRCC magnitude.

The results of sensitivity analysis can be used to identify which interactions or processes in a system are important to different observed behaviors, i.e. which of several processes dominates at a particular time. In addition, the results can be used to identify potential targets for therapeutic intervention, e.g. one could target a pathway to which cell behavior is sensitive as identified by sensitivity analysis. For a complete review on uncertainty and sensitivity analyses see (Marino S, Hogue I, Kirschner D, submitted).

Models

Here, we present four different models developed to capture antigen presentation processes at the four different biological scales (*Fig. 1*, *Table 1 panel B*).

Algorithms for predicting pMHC binding affinities

Peptide binding to MHC is a prerequisite for antigen presentation and the event most likely to be affected by polymorphisms that exist within the MHC of human populations. From a clinical perspective, these polymorphisms may distinguish individuals who succumb to a particular infectious disease from those who remain healthy, and significant effort has been expended to assess whether binding occurs between relevant pMHC combinations. However, the sheer numbers of possible peptides (20^9 or approximately 10^{11} peptides of length nine) and MHC molecules (more than 2200 known HLA alleles) make this task all but impossible for anything more than a small sampling of the pMHC combination space.

To circumvent this difficulty, computational algorithms have been developed to predict whether binding occurs between particular combinations of peptide and MHC (*Fig. 4A*). In general, these algorithms have the same aim as other algorithms in bioinformatics: to identify patterns in sequences that are known to either possess or not possess a particular trait. In this case, the trait is binding to a particular MHC molecule.

With this aim in mind, computational algorithms have been built around a number of statistical and machine learning methods to predict pMHC binding (*Fig. 4A*). The first and simplest algorithms were based on the identification of motifs within peptides binding particular MHC (103). An example of such a motif is the requirement for a hydrophobic amino acid at the N-terminus (position 1) of a 9mer binding MHC of the DR1 serotype, a guideline still generally followed today (16). The advent of competitive binding assays allowed a more nuanced view of binding to be taken. Motifs that required certain amino acids to be present in MHC-binding peptides were superseded by matrices scoring amino acids at each position within the peptide. Different statistical methods could be used to generate the elements of the matrix, including non-linear and linear programming (104, 105), stepwise discriminant analysis (106–108), and partial least squares (109, 110). One simplifying assumption made in many of these algorithms is that binding of each amino acid within the peptide to the MHC molecule occurs independently of adjacent as well as more distal amino acids. Although this assumption was largely confirmed by available crystal structures, algorithms were also developed that did not rely on this assumption based on machine learning methods. Several machine learning methods have now been incorporated into prediction algorithms including artificial neural networks (111–113), hidden Markov models (114), and support vector machines (115, 116).

A different approach has been used to predict the structure of the pMHC complex and attempted to calculate the free energy change (117–121). Structure-based prediction may someday supplant statistical or machine learning-based algorithms but is currently hampered by the limited availability of solved structures and high computational costs. For a more comprehensive review of algorithms, the reader is referred elsewhere (122, 123).

An obvious question to ask about the preceding list of algorithms is how well each one performs compared with the others. To gauge prediction accuracy, an algorithm that has been trained on a set of data is used to make predictions on a test

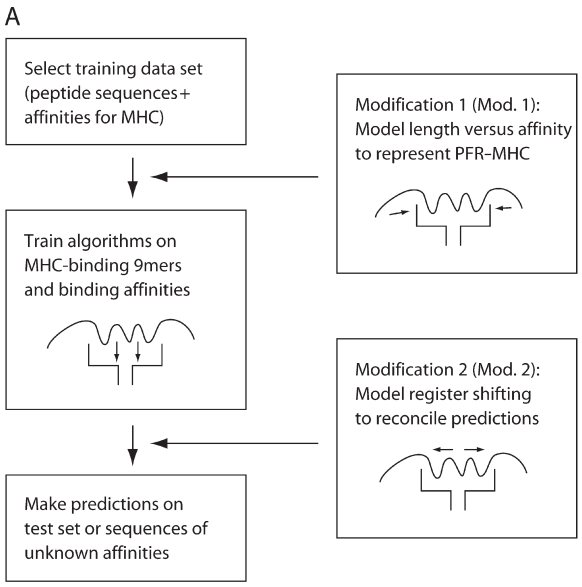

B

	DRB1*0101	DRB1*0401
ISC-PLS (reference algorithm)	0.615	0.730
Mod. 1: Affinity-length model	0.754	0.741
Mod. 2: Register shifting model	0.709	0.757

Fig. 4. Algorithms to predict pMHC binding. (A) On the left, we show three steps common to most algorithms: training data selection, algorithm fitting or training, and testing. On the right, we show two modifications that we have proposed making to these algorithms to improve prediction of longer peptides (i.e. those greater than nine amino acids in length). These modifications are intended to account for PFR–MHC interactions and register shifting. (B) Performance of one published algorithm, ISC-PLS (110), before and after modifications proposed in (A), on training and test sets for two MHC II alleles as measured by Aroc.

data set for which affinities are known, and the output of the algorithm is compared with the known affinities (*Fig. 4A*). A score is then calculated to determine how closely predicted affinities approximate known affinities; however, this task is complicated by differences in the nature of algorithm output. In some cases, output is a continuous variable (affinity), while in other cases, it is discrete (binding or non-binding). This reflects differences in the nature of the available binding data on which these algorithms are fitted or trained. Some databases provide only lists of peptides that either bind or do not bind particular MHC variants (124), while other databases provide a measure of affinity such as IC_{50} (20). The appropriate performance measure therefore differs according to whether input and output are both continuous (Pearson correlation coefficient), both discrete (Matthews correlation coefficient), or discrete and continuous, respectively [area under receiver operating characteristic curve (A_{ROC})]. The A_{ROC} plots represent the probability of true positives versus false positives, given a particular threshold or cut-point for a discriminatory test. A completely random outcome would have an area = 0.5, while a test that perfectly discriminates (detects all true positives and no false positives) would have an area = 1.0. As with PRCC, these correlation coefficients vary between −1 and 1, while A_{ROC} ranges from 0.5 to 1.0. In both cases, higher scores indicate more accurate predictions. Continuous data can be converted into discrete data by assuming that a certain threshold affinity is required for binding, such as an IC_{50} of 500 nM (21), allowing some overlap between performance measures. Examples of scores obtained for several algorithms are provided in MHCBench (125). For example, using binding data for the human MHC II allele HLA-DRB1*0401 from which homologous sequences had been removed, twelve algorithms were found to produce A_{ROC} scores between 0.57 and 0.76.

Our efforts in this area have focused on improving how prediction algorithms handle features that distinguish MHC II-binding peptides from MHC I-binding peptides. Because peptides binding MHC I lack the heterogeneity in peptide length characterizing MHC II-binding peptides, most prediction algorithms were originally developed in the context of MHC I. Adapting these algorithms to MHC II therefore requires an assumption to be made regarding how heterogeneity in length affects binding. One possibility is that parts of the peptide extending past the ends of the MHC II peptide-binding groove, the so-called peptide-flanking regions (PFRs), interact with more distal areas of the MHC molecule (126). In most algorithms, it is assumed that PFRs do not interact with the MHC molecule and have a negligible effect on binding. In addition, longer peptides are also more likely to have additional binding registers (9mer subsequences that fit in the binding groove), allowing shifting among the registers. Some algorithms assume that the highest affinity register predominates (18, 127). Other algorithms assume that all registers are presented in equal numbers and predict the measured binding affinity to be the mean affinity of the different registers (110). We have proposed instead that registers are presented in quantities proportional to their equilibrium affinities and that the measured affinity of a given pMHC complex therefore represents a weighted average (180), a situation analogous to competition between receptors of different affinities for ligand (90).

We hypothesized that the effects of PFR interactions and register shifting could be discernible in plots of affinity versus length and could be taken into account either by filtering the data prior to use in algorithm fitting or training (in the case of PFR–MHC interactions) or by using an equation for register shifting (*Fig. 4A*). Recently, we have shown that both modifications significantly improve the performance of multiple algorithms (180). In *Fig. 4B*, the results of our modifications for one such algorithm, ISC-PLS (110), applied to two MHC alleles are shown. These results are consistent with those of past experimental studies showing that peptide length affects binding to a number of MHC alleles (128, 129).

The output of these computational algorithms is a prediction of binding between particular peptides and MHC alleles, one measure of which is the equilibrium dissociation constant of a pMHC complex (K_D) or the related IC_{50}. (In the remainder of this review, we use the term affinity to refer to the reciprocal of K_D, so that higher affinity refers to stronger binding). Affinity is one of several parameters that determine the number of pMHC displayed on the surface of the APC. To understand the role that cellular parameters also play in determining pMHC display, we next turn to models of the APC.

Models for antigen processing and presentation by APCs

pMHC binding is only one step of many that constitute the antigen presentation pathway, and other steps may confer additional specificity to or alter the dynamics of which peptides are ultimately presented (*Fig. 2*). In both MHC I- and MHC II-mediated antigen presentation, antigens are acquired (from either an intracellular or an extracellular source), degraded into peptides (i.e. processed), and trafficked to the cell surface after binding MHC. At the same time, MHC molecules are synthesized, trafficked to and from the surface, and degraded. Many of these steps are subject to complex regulation by the cytokine environment and feedback signals. The peptides found to bind a particular MHC variant may therefore only provide

a rough, static approximation of peptides that are ultimately presented in a dynamic fashion.

Models of antigen presentation must therefore account for more than pMHC binding. In the case of MHC I-mediated antigen presentation, at least two additional events are known to confer selectivity: proteasomal cleavage and TAP transport. Algorithms have been developed to predict which peptides progress through these stages, and only recently, have they been daisy-chained together with algorithms of pMHC binding to represent antigen presentation *in toto* (130, 131). The result is a more accurate but still static picture of the peptides encountered by $CD8^+$ T cells.

In contrast, we were initially interested in the dynamics of MHC II-mediated antigen presentation but not necessarily in its specificity. To track the levels of different molecular intermediates in the pathway, we used a mathematical representation known as ordinary differential equations (ODEs). ODEs are commonly used to represent systems that are both continuous and deterministic. One assumption made in using ODEs is that the represented entities exist as large, well-mixed populations (i.e. can be approximated as continuous). For MHC II-mediated antigen presentation, the available data validated this assumption. Baseline estimates of the number of MHC II molecules expressed by APCs were on the order of 10^5, and antigen was typically present at high concentrations, at least *in vitro* ($>10^{12}$ peptides per cell) (82, 83). Furthermore, precedent for using ODEs had been provided by models of receptor–ligand systems of which pMHC could be considered one instance (90).

Using a series of models that have incorporated increasing amounts of biological detail, we have been able to address different aspects of antigen presentation that have not always been tractable in the laboratory setting. The first model included only those intracellular processes believed to be essential for antigen presentation (antigen uptake and processing, pMHC binding, and MHC trafficking and recycling) but was sufficient to generate realistic time courses of pMHC levels on the APC surface of both macrophages and B cells (132). Parameters that would have been difficult to manipulate experimentally, e.g. the rate of antigen uptake, were easily varied in the model. The relationship between these parameters and the level of antigen presentation could then be studied without concerns of inhibitor toxicity. Later versions of this model included self-peptides and TCR and expanded the range of questions that could be asked: at what density are exogenous peptides presented relative to self-peptides (133), and can higher pMHC affinity offset lower pMHC–TCR affinity to engage the same number of TCRs (41)?

In the latest version of this model, we have included the regulatory effects of IFN-γ to more closely mirror experimental protocols used *in vitro* (134) (*Fig.* 2). For parameters that were unique to this model, values were either derived from the recent literature or constrained by biological requirements (e.g. to maintain low-level MHC expression in resting APCs, as observed experimentally). The model was tested by comparing the dynamics of several output variables to experimental data. For example, times at which CIITA messenger RNA (mRNA) and MHC II mRNA reached maximal levels following IFN-γ stimulation were compared in simulation and experiment and found to be similar (*Fig.* 5*A,B*). The final model contained 16 variables, each representing a different molecular species, and 30 rates or rate constants.

This model was developed initially to explore presentation dynamics in macrophages. However, with appropriate parameter values, it can be used also to simulate pMHC display by DCs. Because DCs have an enhanced capability for antigen uptake and greater numbers of MHC available (135, 136), they display more pMHC on their surfaces than macrophages (*Fig.* 5*C*).

There were several key findings of our model. First, the number of cell surface pMHC was calculated and shown to be a strong function of a molecular-scale parameter, pMHC affinity (*Fig.* 5*D*). This finding is relevant to the linking of individual models (here, molecular and cellular scales) toward producing a multiscale representation of antigen presentation. Second, sensitivity analysis showed that particular cellular parameters may have increasing or decreasing effects on pMHC levels over time (*Fig.* 5*E*). For example, the effects of varying rates of MHC transcription are only apparent at longer time scales (here, 10–100 h), while the effects of varying trafficking of pMHC to the cell surface play a more prominent role early in the process (1 h), showing how the importance of a particular intracellular process to surface pMHC levels can be time dependent.

Models of cell–cell interactions in the LN

Our focus thus far has been on molecular and cellular events involved in antigen presentation. Here, we examine the interactions between cells of the immune system and place these dynamics in the context of the environment that houses the majority of antigen presentation activities: the LN. This examination not only allows us to bring another key biological scale into our model – that of tissue – but also brings us closer to the goal of developing a full-system model of antigen presentation and its role in the immune response.

There have been numerous mathematical models studying the interactions of immune cells (reviewed in 137). Most of these earlier models of cellular dynamics were built on ODE

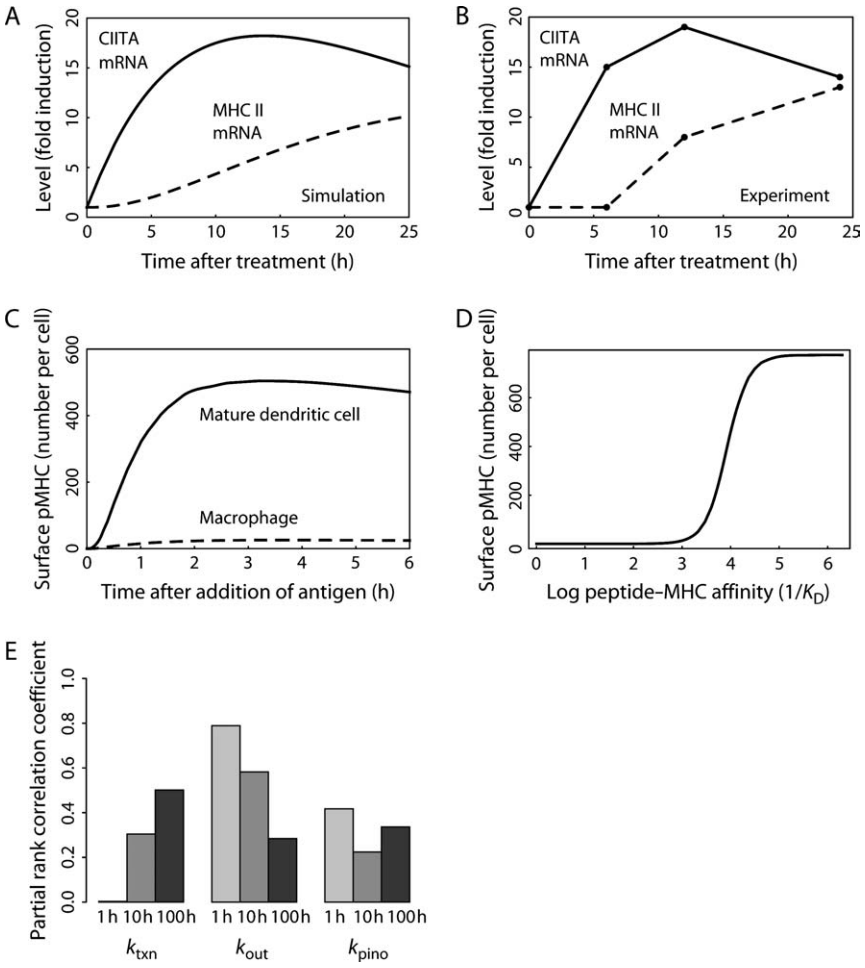

Fig. 5. Model of a single APC. ODEs were written based on the events shown in Fig. 2. (A) Model simulation of CIITA mRNA and MHC II mRNA levels in macrophages following IFN-γ treatment representing a positive control. (B) Experimental data (179) for comparison with (A). (C) Comparison of the antigen-presenting abilities of macrophages and DCs. Macrophage parameter values (i.e. baseline) were taken from Chang *et al.* (134). Two parameters were changed to simulate DCs: rate constants for uptake and MHC II expression (135, 136). (D) Number of surface pMHC complexes as a function of pMHC affinity ($1/K_D$) in macrophages 3 h following addition of antigen. (E) PRCCs for three parameters (k_{txn}, k_{out}, k_{pino}) at three time points (1, 10 and 100 h following addition of antigen). k_{txn}, MHC II transcription rate constant; k_{out}, rate constant for trafficking of pMHC to the cell surface; k_{pino}, pinocytosis rate constant.

systems that were continuous and deterministic in their abstraction of cellular events. Typically, the LN is not explicitly included; however, when it is considered, it is treated as a coarse-grained (i.e. with little mechanistic detail), well-mixed compartment and the spatial structure is disregarded.

We are currently exploring the dynamics of antigen presentation within the LN using an agent-based model (ABM) approach (S. Bajaria *et al.*, manuscript in preparation, T. Riggs *et al.* manuscript in preparation). ABMs are algorithm- or rule-based models that allow for a discrete and stochastic representation of cells and events (89). In an ABM, cells (or any other entity of interest) are represented as discrete software objects (or 'agents') and placed on a lattice. Rules are assigned to the agents governing their movement and interactions within the lattice that represents the LN in our model. A time step is then specified for the model, based on considerations of durations of cell movements and interactions (e.g. 1 min to move one cell length), and the model is run for as many time steps as desired. ABMs therefore have the following components in common: (i) agents; (ii) the environment where agents reside; (iii) the rules that govern the dynamics of the agents; and (iv) the time scales on which these rules are executed. We describe below each of these components as they are represented in our model.

The goal of our model was to understand how the interactions of individual APCs and T cells within the specific spatial and chemical environment of the LN generate observed numbers of activated T cells. An ABM is useful here, as it allows tracking of individual APCs and their interactions with both T cells and their environment. ABMs can also capture spatial aspects of the system, for example the particular geometry of the LN and any groupings of cells that develop. These features are not readily available in the more commonly used differential equation formulations. Another advantage of ABM over ODE model representations is the opportunity to observe how outcomes are influenced by various stochastic events that are not wholly deterministic. We do note, however, that a disadvantage of ABMs as a model framework at this early stage in their development is a shortage of rigorous analysis techniques; models tend to be highly specific and parameter dependent. Furthermore, because stochastic events influence

the outcome, a large number of simulations are required to characterize the mean behavior of the system. In a recent study by our group, we compared four different modeling techniques to explore a different immunological problem – how a granuloma (a spheroid mass of APCs, T cells, and bacteria) forms during *Mtb* infection – and while each of the approaches made important and consistent predictions, the ABM yielded the most realistic results (138).

The agents in our model are the cells known to participate in antigen presentation events. In our initial studies, we have included $CD4^+$ and $CD8^+$ T cells and DCs. Because this model captures only a single LN, we used phenomenological source functions describing the entry of cells to the LN. We count cells as they exit the LN as well but do not track them further.

The spatial environment of our model consists of a two-dimensional (2D) lattice with 100 microcompartments, each of size 20×20 μm and together large enough to represent a single human LN (*Fig.* 3). T cells and DCs interact in the LN paracortex, a region facilitating communication between the immune mediators, such as cytokines, and the cells that they influence (56). Each microcompartment is designed to hold only one DC, the largest cell in the system. Up to two T cells can share the same microcompartment, and multiple molecules (e.g. cytokines and antigen) can also be found in each microcompartment. A 2D representation is reasonable for ease of computation. Also, analysis of multiphoton microscopy data from 2D cross-sections indicates that the majority of dynamic behavior occurs in the 2D plane and only occasionally do cells jump to other depths (out of the plane of observation) (57, M. Miller, personal communication).

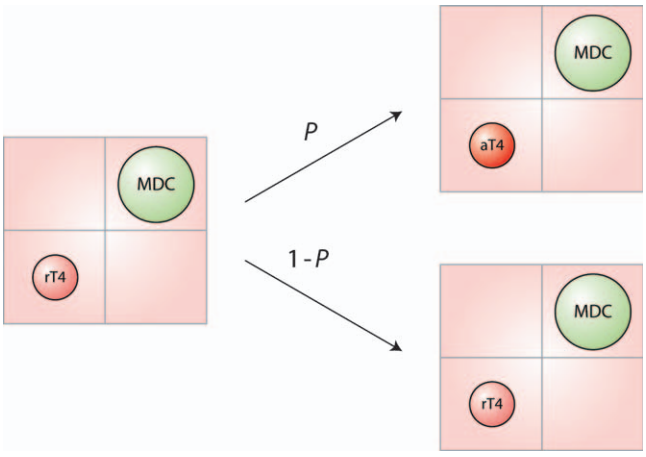

***Fig. 6.* Rule for T-cell activation within the ABM.** If an MDC and a resting (and naive) $CD4^+$ T cell (rT4) are in neighboring microcompartments, then there is a probability P that the resting cell will become activated.

Also included as part of the environment are antigens (whether non-specific or from a particular bacterium or virus) and cytokines/chemokines such as IL-2. These are all treated as continuous variables that are real valued in each microcompartment of the lattice. Treating molecules in solution as continuous variables is reasonable, as the concentrations of these molecules are high in comparison with cell numbers.

Discrete agents in the model are assigned a set of states and rules. As an example, a $CD4^+$ T cell can have one of three states: resting (and naive), activated, or effector. They also have a lifespan. For each state, rules are specified governing the interactions possible for that state. One such rule is the following (*Fig.* 6): if a mature DC encounters and binds a resting $CD4^+$ T cell in one of eight neighboring microcompartments for 15 h (139), then the $CD4^+$ T cell becomes activated with probability p. (Note: Because two T cells can occupy one microcompartment, this means that a single DC can bind up to 16 T cells at one time.) For each implementation of the rule, a number is drawn from a uniform distribution with range [0, 1], and when the chosen number is less than the parameter value, e.g. $p = 0.25$, then the event occurs. Otherwise, it does not. (This again illustrates the contrast between a deterministic versus ABM implementation of a probability rule.) Predictions using different probabilities of activation can be generated, and the effect on the system can be examined using sensitivity analysis. Other rules account for the ability of DC dendrites to scan neighboring compartments for cognate T cells, allow a resting T cell to remain bound to a DC for 10–15 h while becoming activated, and allow a MDC to bind up to 16 T cells, as observed in microscopy studies (71, 63). The rules for APC–T-cell interactions in this model are flexible and can accommodate many different lines of experimental evidence regarding how these cells interact. The time step used for updating cell position was 2 min. Other time-dependent phenomena included lifespan of cells, duration of cell binding, and recruitment of new T cells through the HEV.

Simulations of a number of different conditions were performed. The negative control depicts simulations in the absence of antigen. In this case, immature DCs and resting $CD4^+$ T cells are present in homeostatic numbers (data not shown). *Fig. 7A* shows T cells and DCs in the LN at a single time point (approximately 42 h) of the simulation after the arrival of six MDCs from a site of infection. What is evident for the first time using our model is a spatial organization to the dynamics of antigen presentation. For example, in *Fig. 7A*, clusters of DCs and T cells are seen. Such clusters are necessary for activation of T cells as well as for licensing of MDCs (63). As in the

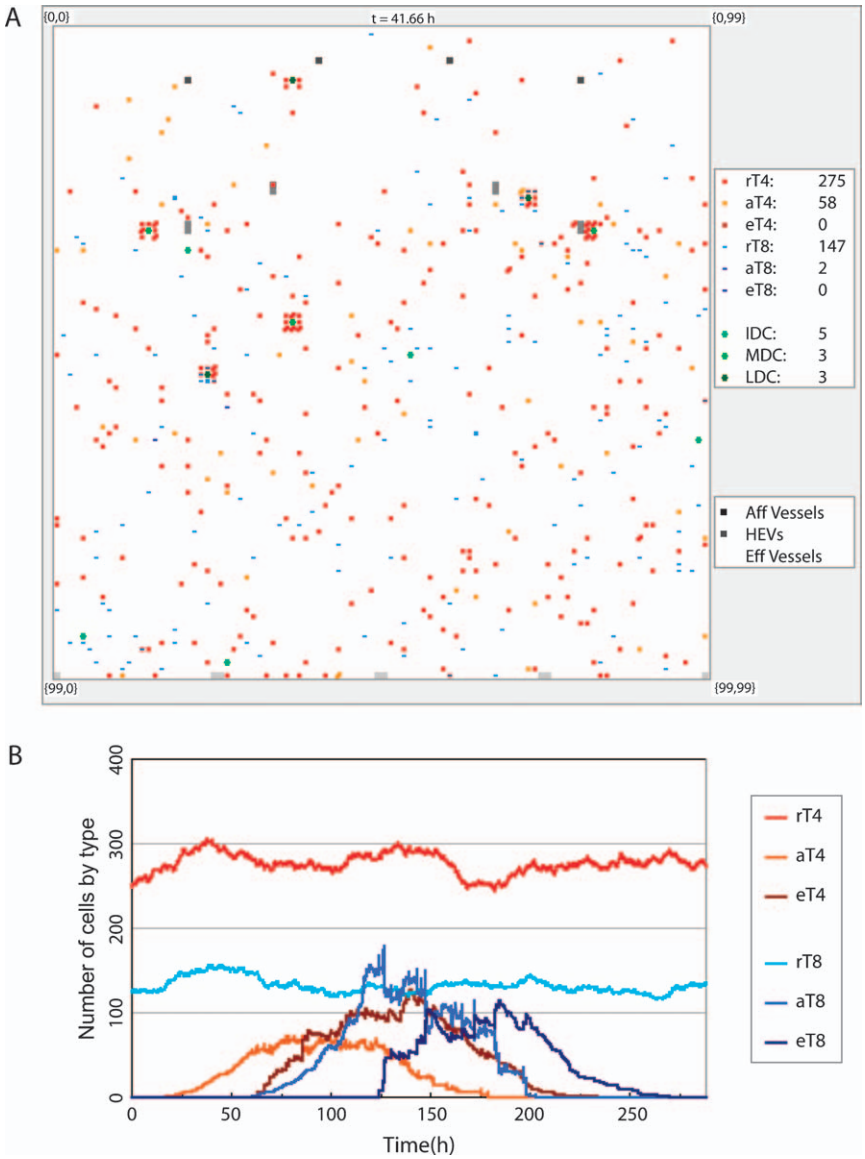

Fig. 7. Cell dynamics in the simulated LN. (A) Snapshot of cells in the LN at ≈42 h after introduction of six MDCs onto the ABM lattice at day 0 of the simulation. Initial conditions were 250 resting $CD4^+$ T cells, 125 resting $CD8^+$ T cells, and 5 immature DCs. A complete list of rules are provided elsewhere (Bajaria *et al.*, manuscript submitted). (B) Temporal dynamics of all cell populations in the simulation. Cell types are as defined in *Fig.* 3.

microscopy, we observe that these clusters move and conjoin (M. Miller, personal communication).

To track the total sizes of the cell populations as they evolve over time, snapshots such as that shown in *Fig. 7A* are enumerated for each cell type. *Fig. 7B* shows the temporal dynamics of each of the cell populations over the entire time frame of the simulation and indicates the following course of events for T-cell dynamics over the simulated infection. With the introduction of only six mature, antigen-bearing DCs on day 0 (into a system that is already in homeostasis), we see an increase in activated $CD4^+$ T cells (aT4) and then a day or so later a similar increase in effector $CD4^+$ T cells (eT4). Effector $CD4^+$ T-cell numbers peak at approximately 6 days (approximately 140 h), 2 days after activated $CD4^+$ T-cell numbers peak. Both decline slowly after that. This is expected as immature DCs have a lifespan in the range of 1–9 days, MDCs have a lifespan of 3 days, and LDCs have a lifespan of 1.5 days. (In the model, LDCs are MDCs that have engaged a $CD4^+$ T cell for a long period of time or after having engaged an effector $CD4^+$ T cell). No additional MDCs were introduced in this simulation. $CD8^+$ T-cell numbers follow a similar path, and in addition, memory cells are generated. Note that the levels of resting $CD4^+$ and $CD8^+$ T cells remain in homeostasis even during this infection scenario. This result emerges from the model and represents a natural feedback regulation that occurs. Thus, while cells are being recruited to the other subclasses (i.e. through activation), new cells continue to enter into the LN to replace them, maintaining homeostatic resting T-cell numbers and supplying new T cells that can be recruited to an activated state.

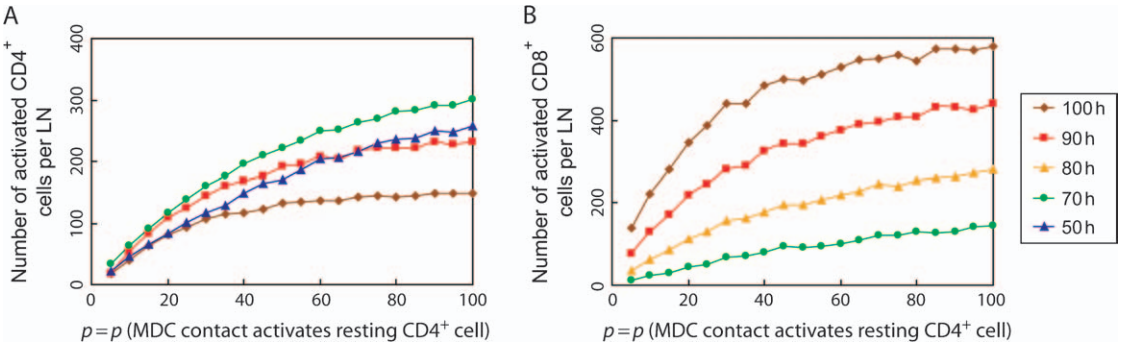

***Fig. 8.* Effect of variation in the probability of activating resting CD4$^+$ T cells in the ABM.** The parameter *p* represents the probability of activation of a resting CD4$^+$ T cell upon interaction with a cognate MDC and is varied from 0.05 to 0.95. (A) The number of activated CD4$^+$ T cells produced at a given time point increases with *p*. (B) Likewise, the number of activated CD8$^+$ T cells produced at a given time point also increases with *p*. In this Figure, 16 MDCs were introduced on day 0.

To illustrate the usefulness of sensitivity analysis in this setting, we explore the parameter representing the probability that binding between a CD4$^+$ T cell and its cognate MDC results in activation of the T cell. As discussed above, T-cell activation likely depends on many factors including the number of pMHC on the surface of the DC as well as the binding affinity between pMHC and TCR. In our ABM, these factors are combined into the representative parameter *p*. *Fig.* 8 shows a dynamic plot of two model outcomes, the number of activated CD4$^+$ (*Fig.* 8*A*) and activated CD8$^+$ T cells (*Fig.* 8*B*) in the LN versus *p* (the probability that a CD4$^+$ T cell becomes activated upon encounter with an MDC or LDC) at four time points. In both cases, activated CD4$^+$ and CD8$^+$ T-cell numbers increase as a function of *p*. Activation of both cell types is a strong function of *p*, and this could be explored further by integrating finer detail in this term (i.e. by incorporating the smaller length scale models described previously), a first step at a multiscale approach.

The ABM allowed us to obtain information regarding individual cell behavior for different cell types. This approach was in many ways superior to that of continuous models for the questions we were exploring here. First, we could track the location and state of all cells at any given time point, allowing determination of spatial dynamics. Second, individual cell–cell interactions could be tracked in both space and time. These features allowed us to make predictions regarding biological mechanisms that were not feasible using continuous model approaches. For example, we determined that the lifespan of LDCs greatly affects the number of effector CD8$^+$ T cells generated (PRCC = 0.75 with *p*-value $< 10^{-6}$). If a therapy could be identified to prolong LDC lifespan, then the model predicts that a greater cytotoxic T-cell response would be generated.

Finally, in the ABM of the LN, we were able to track how many effector cells leave the LN over time. However, the model did not capture the trafficking events of these cells from the LN back to the site of infection, the next important step in the immune response. In addition, the entry of cells into the LN was represented simply, using a single parameter, which does not account for factors such as the amount of antigen initially produced at the site of infection that ultimately limits the number of MDCs. In the next section, we discuss ways to integrate the LN into a more complete model of trafficking of cells during an immune response.

Multicompartment models of the LN with other organ systems

To capture the full spectrum of immune system dynamics in a model, it will be necessary to include physiological compartments in addition to the LN. Immune cells regularly circulate through the blood, and because of ease of access, data on blood are the major diagnostic available to the physician. However, data on blood provide only a snapshot of a system that also includes the lymphatics (which drain the tissues, typically key sources of antigen and DCs) and various organs and sites of infection.

To capture different physiological compartments, a model is usually developed for each compartment separately and then linked to the other models by representing the trafficking of shared elements between the compartments. Most typically, the dynamics within each particular compartment as well as the trafficking between compartments are described with ODEs, although other possibilities exist. Which compartments are included in any particular model will depend on the types of infection being simulated and the questions being asked. For example, in studies on the immune response to *Mtb*, it will be critical to include the lung compartment where granuloma formation occurs. Further, developing models that include these additional compartments will influence the LN model

described above. In that model, phenomenological source functions were used to describe the trafficking of cells into the LN. We also tracked the number of effector cells leaving the LN but did not allow them to continue to play a role in the immune response. Thus, the goal now is to capture more mechanistically the dynamics of those compartments external to LNs. This will bring us one step closer to developing theories regarding overall immune activation as it depends on local antigen presentation events.

Many compartmental models of biological systems and the immune system have been developed (88, 140). Here, we review two sets of compartmental models developed by our group: the first developed to study HIV-1 infection and the other to study infection with *Mtb*. We present here the non-infection states of these models (i.e. the negative controls) to show that we first describe the dynamics in healthy scenarios (*Fig.* 9). In both cases, the LN is represented along with an additional compartment relevant for disease: the blood in the case of HIV and the lung in the case of *Mtb*.

Our blood–lymph circulation models (*Fig.* 9*A*) were developed first for the case of no infection to observe homeostasis and then in the context of infection, specifically with HIV-1 (141–143). In one study (143), we used ODEs to track $CD4^+$ and $CD8^+$ T cells and DCs circulating within and between the blood and the lymph compartments. The model successfully captures known dynamics of these cell populations in their respective compartments. Dynamics of cell turnover and migration are the main features represented in this model. In the model, $CD4^+$ T-cell counts are about 2×10^{11} in total lymph tissue and approximately 1×10^3 per μl of blood. This finding matches what has been observed in humans (144). The ratio of $CD4^+$ T cells to $CD8^+$ T cells found in the model is 2:1 in both blood and lymph, also as is observed in previous studies (144, 145). We also predicted that there are 10^{11} $CD8^+$ T cells in the lymph system and 5×10^2 $CD8^+$ T cells per μl of blood, which agrees with data from Haase (144). The model also maintains a level of 14–20 DCs per microliter of blood (146).

Our LN–lung compartmental model (*Fig.* 9*B*) is an example of a model that includes both the LN and an additional site of infection, the lung. Effector T cells generated in the LN by antigen presentation leave and travel to particular sites. For this model, which was developed with application to tuberculosis, the site of interest was the lung. The process by which effector T cells travel throughout the body is not well characterized and differs greatly depending on where the site of infection is located. The LNs that are typically involved are the closest draining LNs to the site of infection, facilitating ease of trafficking between compartments.

As in the blood–lymph model, the simplest model here tracks only homeostasis of T cells and DCs between both compartments (72, 73). Specifically, we linked a coarse-grained model of the LN based on a system of ODEs with an existing

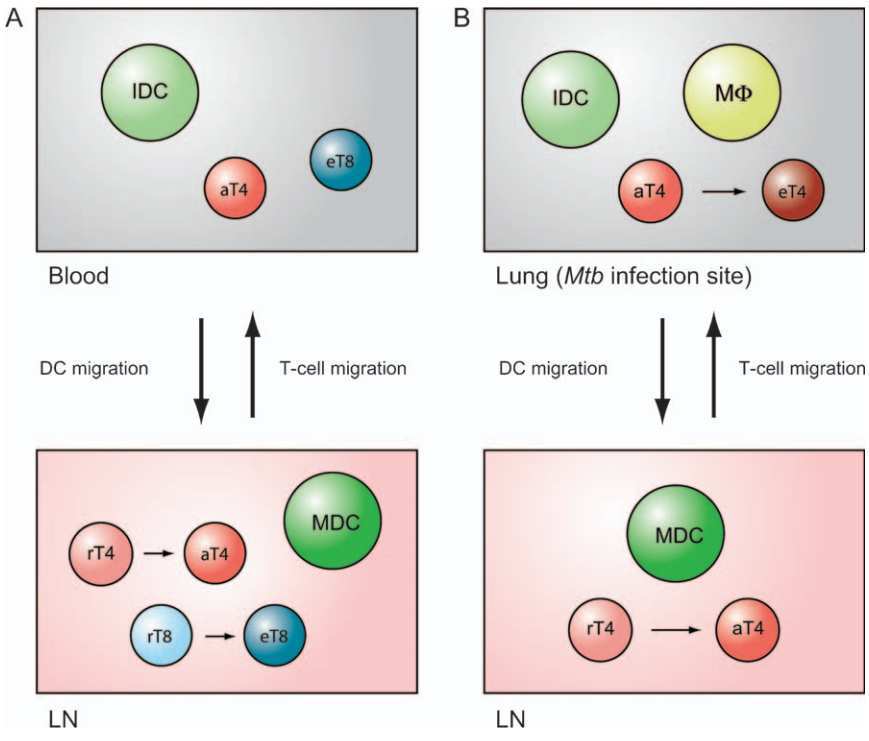

Fig. 9. Two-compartment models of LN linked to another system. (A) LN–blood model. $CD4^+$ T cells, $CD8^+$ T cells, and DCs traffic between these two compartments. (B) LN–lung model. DCs, macrophages (MΦ), and $CD4^+$ T cells traffic between these two compartments. Cell types are as defined in *Fig.* 3. IDC, immature DC.

fine-grained ODE model (i.e. a model that includes many mechanistic details) of the immune response in the lung. In the lung model (147), we tracked resting, infected, and activated macrophages; T-helper (Th) 0, Th1, and Th2 lymphocytes; the cytokines IFN-γ, IL-12, IL-4, and IL-10; and the level of antigen. Important in this model is the presence of macrophages playing multiple roles as APCs, cytokine producers, and killers of intracellular pathogens. In the coarse-grained LN, we tracked MDCs, resting T cells, Th0 cells, and the concentration of the cytokine IL-12 (a promoter of Th1 immunity). To investigate DC trafficking, we modified the lung compartment by including immature DCs in the lung model. In the absence of antigenic stimulation, i.e. at homeostasis, the LN compartment has an average of 10^4 naive, resting $CD4^+$ and $CD8^+$ T cells, and all other cell types are absent. In the lung, there are 5×10^4 immature DCs (approximately 10% of resting macrophage population), and all other cell types are absent. Our results are in agreement with lung and LN data from various animal models on the numbers of cells present in healthy subjects (148–156).

Applications of the individual models to study infection

Each of the individual scale models described above can be used to answer questions and suggest new experiments aimed at uncovering the roles that parameters (representing biological mechanisms) play in antigen presentation at each particular scale. Several examples are given below.

We used the model representing a single APC (*Figs 2 and 5*) to investigate why multiple mechanisms had been proposed to explain how *Mtb* inhibits antigen presentation in macrophages (134). Some researchers had identified MHC II transcription as a process that *Mtb* disrupts in macrophages. Others had suggested antigen processing or pMHC colocalization as targets. By varying the rates or rate constants for particular processes in the model, we were able to predict the effect of the corresponding mechanisms on surface pMHC levels under different experimental conditions. We found that mechanisms could generally be categorized according to the timing of their effects. Targeting antigen processing or pMHC colocalization, for instance, resulted in an immediate decrease in the ability of macrophages to present antigen, while mechanisms targeting MHC expression required a delay of at least 10 h to become effective. However, the stimulatory effects of IFN-γ may necessitate the use of long-term mechanisms by a pathogen, particularly a slow-growing one such as *Mtb*. These two categories of mechanisms can therefore be thought of as non-redundant in function, suggesting that *Mtb* gains distinct benefits from inhibiting multiple intracellular processes.

Sensitivity analysis can be used to identify other possible mechanisms used by *Mtb* to inhibit antigen presentation. Because antigen presentation is required to resolve most infections, the results can often be applied to other pathogens as well. For example, surface pMHC levels were found to be sensitive to the rate constant for pMHC trafficking to the surface at early time points (i.e. <10 h post-infection, *Fig. 5E*). This process as well as others that have more significant effects early relative to cellular scale events may make attractive targets for inhibition by pathogens with shorter doubling times. (Targeting transcription of MHC, in contrast, may require many hours to hinder antigen presentation.) Thus, one way in which anti-microbial therapies could be improved is through ensuring that the pathogenic mechanisms targeted therapeutically are consistent with the time scale of the pathogen's lifetime.

Other examples of applying the individual scale models build on our two-compartmental studies (*Fig. 9*). Our group and others have used multiple compartment models to study infection dynamics. The first models were developed to understand HIV-1 infection (157–159). Studies by our group looked in detail at the dynamics of circulation and trafficking of immune cells in blood and lymphatics during HIV-1 infection (141, 143). The latter model consists of a system of non-linear ODEs that captures interactions between T cells and DCs and builds directly on the LN–blood model discussed above (*Fig. 9A*).

When HIV-1 is introduced into the system, additional cell types must be tracked. HIV-1 infects $CD4^+$ T cells, so there is an additional class: infected cells. Further, because antigen is present, effector $CD8^+$ and $CD4^+$ T cells are generated in response to antigen presentation activities. Simulating this two-compartmental infection model yields good agreement with clinical data in both compartments. In the LN, resting $CD4^+$ and $CD8^+$ T cells both are estimated to be 10^{10} in number, while virus is 9×10^{10} and infected cells are 4×10^9, similar to the results in humans (144). In the blood, activated $CD8^+$ T cells are estimated to be 8.8% of total $CD8^+$ T cells, which is in the same range as observed in previous studies (160, 161). Our model predicts the ratio of activated to total $CD4^+$ T cells in the blood to be approximately $1{:}10^8$, while the only available data suggest that this ratio is roughly $1{:}10^3$. Our prediction varies depending on the level of interaction with DCs (143). When the fine-grained models described above are linked with this model, we should be able to better elaborate the mechanisms of $CD4^+$ T-cell decline during HIV-1 infection and better understand the role that antigen presentation plays.

We have also developed two-compartment models describing *Mtb* infection. Here, we captured the dynamics of a specifically infected tissue (i.e. lung) and its closest associated LN, building on the LN–lung model discussed above (72, 73) (*Fig. 9B*). In addition to the variables included in the homeostasis lung model, we tracked both intracellular and extracellular load of *Mtb*. Once bacteria are present in the system, macrophages can take up bacteria at the site of infection and are classified as infected. If time passes and they are not activated sufficiently to clear their intracellular bacteria, then they are classified as chronically infected. Immature DCs that take up bacteria in the lung traffic to the LN to present antigen and generate effector cells that can now migrate back to the lung to participate in the adaptive immune response.

The model output qualitatively captures the main dynamics of a non-human primate infection model in both lung and LN compartments (72, 73). The measured unit of the model is number of cells (or bacteria) per cm^3 of granulomatous tissue. Total $CD4^+$ T-cell counts during latent tuberculosis range between 1×10^3 and 1×10^4 (both in the lung and in the LN compartment) in the mathematical model. DC numbers during latent tuberculosis range in the lung between 2×10^4 and 2.5×10^4 in the mathematical model (a range similar to that in non-human primates). The main result of this work is that delays in either DC migration to the LN or T-cell trafficking to the site of infection can alter the outcome of *Mtb* infection, defining progression to primary disease or latent infection and reactive tuberculosis.

How to build a multiscale model

Models developed at individual physiological scales can be linked to form a multiscale model. Both mathematical/computational and biological issues bring complexity to this task; the development of efficient and computationally feasible multiscale methods is an area of current investigation (7, 162, 163).

One of the simplest ways to link models is to have the output from one model be the input to another. Coveney and Fowler (164) and Vlachos (162) review an approach in which the results from a model developed at the smallest scale are passed to the model at the next scale, and so on, termed a hierarchical, sequential, or serial approach. For example, the output from a smaller scale model may be the calculated value of an important parameter (e.g. affinity) or a set of values (e.g. the number of cells in a given state as a function of time). Even with a hierarchical approach, there are decisions to make. Does the larger scale model contain the entire smaller scale model? If so, computation may be an issue. Further, with any numerical solver, issues of error arise. For each of the individual models, numerical errors may accumulate, and the propagation of these errors by passing them across scales presents significant challenges.

Alternatively, if changes at larger scales affect behavior at smaller scales, for example if there is feedback occurring over multiple biological scales, a hierarchical approach is no longer valid (but may still be a useful starting point), and a hybrid or coupled multiscale approach should be used. It is likely that this approach will nearly always be the case in biology. For example, changes in ion channels in the heart affect overall heart function. At the same time, blocking blood flow in a coronary artery also affects heart tissue at the cellular scale (165).

To begin to build a multiscale model for our system of antigen presentation, we will need to interface the four individual scale models under development and discussed above (*Table 2*) in a hierarchical fashion (*Fig. 10*). We work under the hypothesis that events at each scale (molecular, cellular, tissue, and organ/organism) of the immune system represented in a multiscale model affect the development of the immune response. First, the output of our molecular-scale model, pMHC II affinity, is a critical parameter that serves as an input into our single APC model. This allows us, for example, to explore the effect that MHC II polymorphism may have on pMHC presentation (*Fig. 10A*). Second, the state of an APC agent, in particular the number of pMHC displayed on the surface as a function of time, can be calculated from our single-cell-scale APC model. At this point, we can determine whether differences in pMHC affinity found at the

***Table 2.* Description of each of the four individual scale models**

Scale	Model description	Model inputs	Model outputs
Molecular	pMHC binding model	Training data (peptide sequence, binding affinities)	pMHC II affinity
Cellular	Single APC model	Antigen and IFN-γ concentrations, cellular parameters	Surface pMHC complexes
Tissue	Cellular interactions in a single LN	Antigen concentration, cell numbers, cellular and LN parameters	Number of effector cells exiting the LN
Organ/organism	Two-compartment models of LN + other sites of interest	Antigen; cell numbers; cell, LN and tissue parameters	Pathogen numbers (i.e. viral or bacterial load)

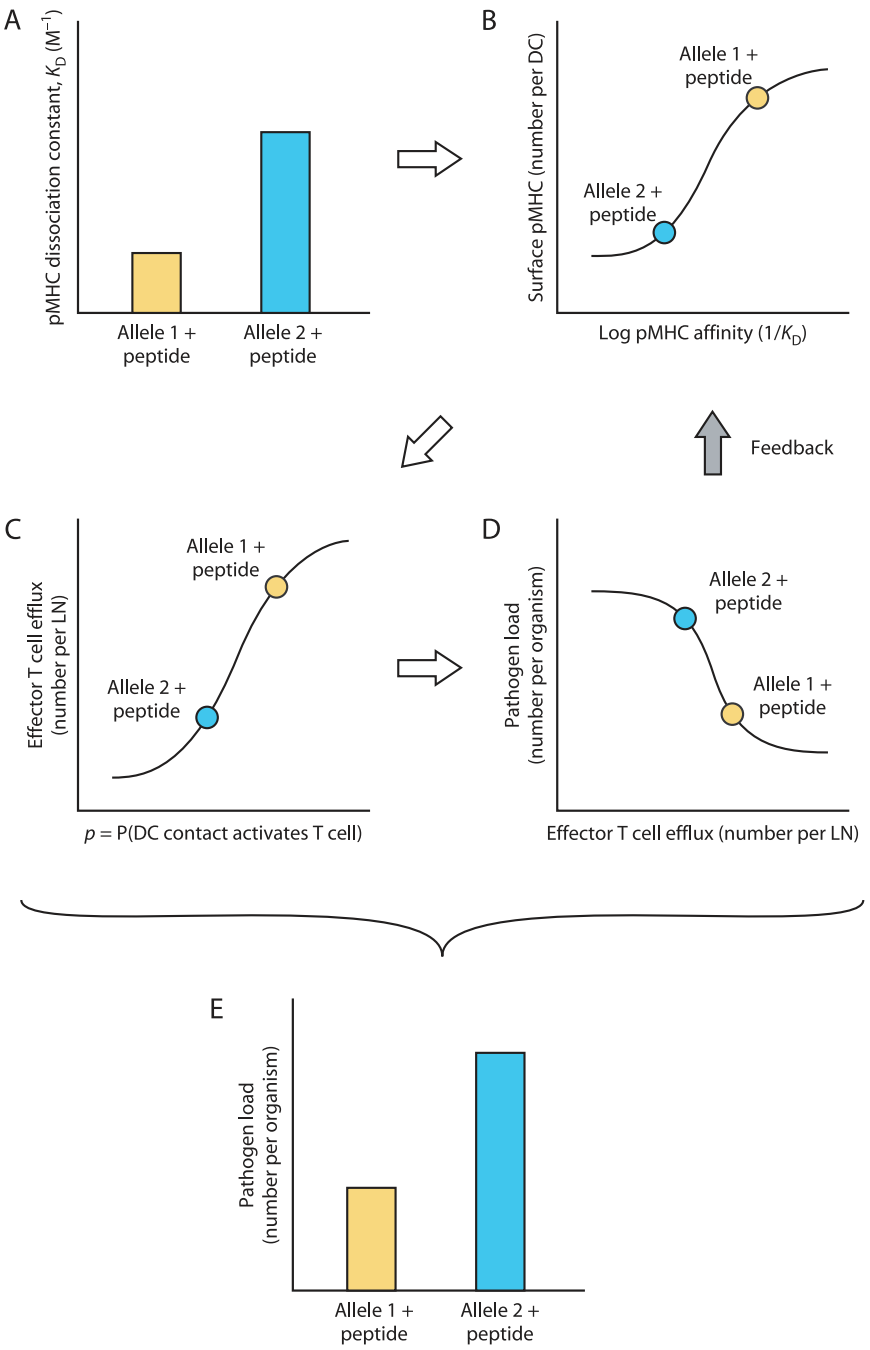

Fig. 10. Building a multiscale model of antigen presentation from four individual scale models. In the particular example shown, the relevance of allele-specific differences in pMHC II affinity to antigen presentation and the overall immune response is explored. Predictions from each scale are fed to the next larger scale model, providing predictions between adjacent (A–D) and non-adjacent (E) scales, i.e. a hierarchical approach is used. A hybrid approach must be used if feedback from larger scales to smaller scales is present, for example if overall pathogen load can affect intracellular events.

smaller scale give rise to significant differences in pMHC display (*Figs 5D and 10B*). Third, the ODE simulations of the APC model will generate individual, single-cell-scale information that will be used to update each agent within the tissue-scale model, the ABM of a single LN. In this model, the number of pMHC complexes on the surface of an APC is currently represented as a probability p that an APC will activate a T cell with which it has come into contact, an input parameter for the ABM. We can now again determine whether differences in pMHC affinity will play a key role, but this time by examining effector T-cell numbers generated in the LN (*Fig. 10C*). Finally, we can use the fairly coarse-grained ODE models developed for particular, relevant body compartments (e.g. blood, sites of infection) together with the fine-grained agent-based LN model to see, for example, the impact of pMHC affinity at the organism scale (*Fig. 10D,E*). One might compare the predictions of this multi-scale model with the data of Geluk *et al.* (25), who showed that only a few *Mtb*-derived peptides elicit a T-cell reaction in mice and that these peptides also bind MHC with high

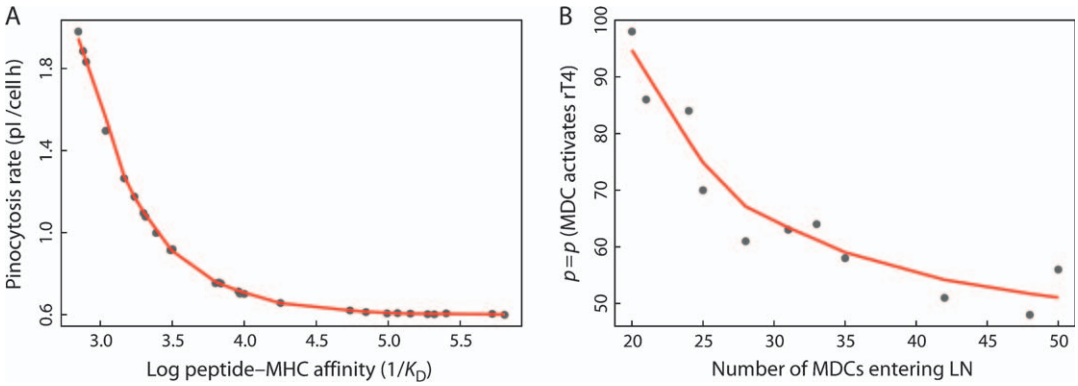

***Fig. 11.* Trade-offs between processes in the models.** (A) The relationship between uptake rate and pMHC II affinity in producing pMHC complexes in the APC model (*Fig. 2*). Each point represents a pair of compensatory parameter values that results in ≈200 pMHC complexes on the APC surface 3 h after antigen is added to macrophages [other parameters were as published in Chang *et al.* (131)]. (B) The relationship between the probability of activation of resting (naive) $CD4^+$ T cells (rT4) versus the number of MDCs that enter the LN on day 0 in generating activated $CD4^+$ T cells in the ABM. Each point represents a pair of compensatory parameter values that results in 330 ± 30 effector $CD4^+$ T cells generated. This result represents the 42-h time point. In both A and B, a local regression line has been fitted to the data.

affinity. Similarly, T-cell proliferation and IFN-γ production have been correlated with pMHC affinity (26). Together, the multiscale model incorporates the molecular, cellular, tissue-scale, and organ/organism-scale models and allows us to explore, among other things, the relevance of pMHC affinity differences to the overall immune response.

In a similar fashion, the impact of combinations of parameters might be explored. For example, can a higher pMHC affinity compensate for poorer APC uptake ability? As shown in *Fig. 11A*, there is indeed such a relationship between affinity and uptake rate. Can a higher pMHC affinity compensate for fewer APCs or fewer highly specific T cells? As shown in *Fig. 11B*, there is a trade-off between the affinity and the number of MDCs required to enter the LN in order to produce a particular number of effector T cells. In *Fig. 11*, affinity is represented as part of the aggregate parameter *p*, the probability that a $CD4^+$ T cell becomes activated after contact with a DC; *p* increases with the number of pMHC displayed, which in turn increases with pMHC affinity (*Fig. 5D*). This finding suggests that an increase in the number of cells presenting antigen within the LN can compensate for a reduced affinity between peptide and MHC or lower numbers of pMHC on the surface of the DC (both factors captured by the probability *p*). A similar result holds for the number of T cells present that can recognize the antigen being presented (data not shown). Thus, although at present, we are still in the early stages of integrating our individual scale models, we can already begin to address some of the multiscale questions posed earlier, in particular those that do not require integration of all four scales.

We described above a hierarchical approach to our multiscale model of antigen presentation. However, at a later stage in model development, we may need to incorporate feedback from larger scales to smaller scales, moving us to a hybrid approach. Information on the local environment in the LN, for example cytokine concentrations, could be passed back to the APC model to allow cytokine concentrations to influence the number of pMHCs on the APC surface. Furthermore, many intracellular pathogens, including *Mtb*, inhibit antigen presentation within macrophages. While the mediators of this effect, including 19-kDa lipoprotein (166–169), act on molecular-scale events within macrophages, the total production of such mediators is likely to depend on the number of pathogens at the site of infection, a tissue-scale quantity. However, the latter quantity can only be predicted after accounting for other tissue-scale factors, such as the activation state of macrophages and Th cells at the site of infection. In this example, then, tissue-scale events feed back on molecular-scale events and *vice versa*.

Once a multiscale model is developed, it can be applied toward the generation of hypotheses regarding the role of antigen presentation in immunity. Recall that there is a clear association between particular MHC alleles and disease susceptibility/resistance. If our molecular scale model shows that there is a link between particular MHC alleles and affinities for particular antigens, then the full multiscale model could be used to show the expected outcome at the system scale (S. Chang, J. Linderman, D. Kirschner, submitted).

As another example, the efficacy of a vaccine is in part determined by activation of $CD4^+$ T cells. A multiscale model

will enable testing of the roles that various factors play in that activation. What is the relationship between antigen dose in the vaccine and the number of MDCs appearing in an LN? What level of T-cell activation is necessary to generate an appropriate memory response (one further possible extension of the multiscale model) that is critical for vaccines to be effective against later challenge? Further, what aspects of the antigen presentation process should be targeted to optimize vaccine efficacy? Can such insights help explain why bacille Calmette–Guérin, the vaccine against *Mtb* used for the last 80 years, has failed to eliminate tuberculosis? Finding the answers to such questions may rely at least in part on the developments described in this review.

Looking ahead

The ultimate goal of developing mathematical/computational models of biological systems is to use these models to better understand the systems and to suggest mechanisms to manipulate the systems, i.e. to treat or prevent disease. For example, one can introduce therapeutic modulation, even modes unapproachable using current medical techniques, in a controlled manner to evaluate potential targets for both treatment and vaccine strategies. Indeed, the US Food and Drug Administration Critical Path Initiative (170) has recently identified model-based drug development, including drug and disease modeling, as an important goal.

There are numerous challenges ahead for the development of multiscale models in biology and for antigen presentation in particular. First, there is a need for experimental data to allow for model validation at every scale. For example, although model development is an essential part to predicting pMHC affinities, the quality and amount of data available to develop models remain an issue (123, 171, 172). The predictive ability of a model should improve with the size of the training set. Currently, databases contain 13 000–24 000 peptides, although the sizes of these databases can be misleading. Laboratories often generate very closely related peptides to determine characteristics of binding; these peptides are then listed as separate entries in the databases. However, using homologous peptides to fit models of pMHC binding can skew predictions. Methods to eliminate homologous peptides are available (173, 174) and, when implemented, significantly reduce data set size.

From a computational perspective, methods for integrating predictions at individual scales and for allowing behavior at each scale to influence behavior at other scales are needed and are currently under development for a number of biological systems (175). In addition, a number of groups are developing platforms with the explicit aim of standardizing models; this development would make it easier to pass models from one research group to another (176–178).

In sum, nearly all biological processes involve multiple scales. Thus, the lessons learned here regarding the use of modeling to integrate molecular, cellular, tissue-scale, and organ/organism-scale events can inform studies on a broad range of biological systems and provide tools to analyze them.

References

1. Savageau MA. Reconstructionist molecular biology. New Biol 1991;**3**:190–197.
2. Hunter P, Nielsen P. A strategy for integrative computational physiology. Physiology (Bethesda) 2005;**20**:316–325.
3. Bassingthwaighte JB, Chizeck HJ, Atlas LE, Qian H. Multiscale modeling of cardiac cellular energetics. Ann N Y Acad Sci 2005;**1047**:395–424.
4. Choe Y. The role of temporal parameters in a thalamocortical model of analogy. IEEE Trans Neural Netw 2004;**15**:1071–1082.
5. Breakspear M, Stam CJ. Dynamics of a neural system with a multiscale architecture. Philos Trans R Soc Lond B Biol Sci 2005;**360**: 1051–1074.
6. Robinson PA, Rennie CJ, Rowe DL, O'Connor SC, Gordon E. Multiscale brain modelling. Philos Trans R Soc Lond B Biol Sci 2005;**360**:1043–1050.
7. Alarcon T, Byrne HM, Maini PK. Towards whole-organ modelling of tumour growth. Prog Biophys Mol Biol 2004;**85**:451–472.
8. Peirce SM, Skalak TC. Microvascular remodeling: a complex continuum spanning angiogenesis to arteriogenesis. Microcirculation 2003;**10**:99–111.
9. Reeves GT, Kalifa R, Klein DE, Lemmon MA, Shvartsman SY. Computational analysis of EGFR inhibition by Argos. Dev Biol 2005;**284**:523–535.
10. Glotzer SC, Paul W. Molecular and mesoscale simulation methods for polymer materials. Annu Rev Mater Res 2002;**32**:401–436.
11. Comisar WA, Hsiong SX, Kong HJ, Mooney DJ, Linderman JJ. Multi-scale modeling to predict ligand presentation within RGD nanopatterned hydrogels. Biomaterials 2006;**270**:2322–2329.
12. De Libero G, Mori L. Recognition of lipid antigens by T cells. Nat Rev Immunol 2005;**5**:485–496.
13. Cheng Y, Prusoff WH. Relationship between the inhibition constant (K1) and the concentration of inhibitor which causes 50 per cent inhibition (I50) of an enzymatic reaction. Biochem Pharmacol 1973;**22**:3099–3108.
14. Sette A, Buus S, Colon S, Miles C, Grey HM. Structural analysis of peptides capable of binding to more than one Ia antigen. J Immunol 1989;**142**:35–40.
15. Roche PA, Cresswell P. High-affinity binding of an influenza hemagglutinin-derived peptide to purified HLA-DR. J Immunol 1990;**144**:1849–1856.
16. Southwood S, et al. Several common HLA-DR types share largely overlapping peptide binding repertoires. J Immunol 1998;**160**:3363–3373.
17. Dedier S, Reinelt S, Rion S, Folkers G, Rognan D. Use of fluorescence polarization to monitor MHC-peptide interactions in solution. J Immunol Methods 2001;**255**:57–66.

18. Brusic V, Rudy G, Honeyman G, Hammer J, Harrison L. Prediction of MHC class II-binding peptides using an evolutionary algorithm and artificial neural network. Bioinformatics 1998;**14**:121–130.
19. Bhasin M, Singh H, Raghava GP. MHCBN: a comprehensive database of MHC binding and non-binding peptides. Bioinformatics 2003;**19**:665–666.
20. Toseland CP, et al. AntiJen: a quantitative immunology database integrating functional, thermodynamic, kinetic, biophysical, and cellular data. Immunome Res 2005;**1**:4.
21. Sette A, et al. The relationship between class I binding affinity and immunogenicity of potential cytotoxic T cell epitopes. J Immunol 1994;**153**:5586–5592.
22. Vukmanovic S, Neubert TA, Santori FR. Could TCR antagonism explain associations between MHC genes and disease? Trends Mol Med 2003;**9**:139–146.
23. Rajagopalan S, Long EO. Understanding how combinations of HLA and KIR genes influence disease. J Exp Med 2005;**201**:1025–1029.
24. Thorsby E, Lie BA. HLA associated genetic predisposition to autoimmune diseases: genes involved and possible mechanisms. Transpl Immunol 2005;**14**: 175–182.
25. Geluk A, et al. Identification of HLA class II-restricted determinants of Mycobacterium tuberculosis-derived proteins by using HLA-transgenic, class II-deficient mice. Proc Natl Acad Sci USA 1998;**95**:10797–10802.
26. Hill JA, Wang D, Jevnikar AM, Cairns E, Bell DA. The relationship between predicted peptide-MHC class II affinity and T-cell activation in a HLA-DRbeta1*0401 transgenic mouse model. Arthritis Res Ther 2003;**5**:R40–R48.
27. Bryant P, Ploegh H. Class II MHC peptide loading by the professionals. Curr Opin Immunol 2004;**16**:96–102.
28. Honey K, Rudensky AY. Lysosomal cysteine proteases regulate antigen presentation. Nat Rev Immunol 2003;**3**:472–482.
29. Denzin LK, Cresswell P. HLA-DM induces CLIP dissociation from MHC class II alpha beta dimers and facilitates peptide loading. Cell 1995;**82**:155–165.
30. Adorini L, Muller S, Cardinaux F, Lehmann PV, Falcioni F, Nagy ZA. In vivo competition between self peptides and foreign antigens in T-cell activation. Nature 1988;**334**: 623–625.
31. Chicz RM, Urban RG, Gorga JC, Vignali DA, Lane WS, Strominger JL. Specificity and promiscuity among naturally processed peptides bound to HLA-DR alleles. J Exp Med 1993;**178**:27–47.
32. Chomarat P, Banchereau J, Davoust J, Palucka AK. IL-6 switches the differentiation of monocytes from dendritic cells to macrophages. Nat Immunol 2000;**1**:510–514.
33. Chomarat P, Dantin C, Bennett L, Banchereau J, Palucka AK. TNF skews monocyte differentiation from macrophages to dendritic cells. J Immunol 2003;**171**:2262–2269.
34. Fogg DK, et al. A clonogenic bone marrow progenitor specific for macrophages and dendritic cells. Science 2006;**311**:83–87.
35. Inaba K, Steinman RM. Protein-specific helper T-lymphocyte formation initiated by dendritic cells. Science 1985;**229**:475–479.
36. Inaba K, Pack M, Inaba M, Sakuta H, Isdell F, Steinman RM. High levels of a major histocompatibility complex II-self peptide complex on dendritic cells from the T cell areas of lymph nodes. J Exp Med 1997;**186**:665–672.
37. Reinhardt RL, Khoruts A, Merica R, Zell T, Jenkins MK. Visualizing the generation of memory CD4 T cells in the whole body. Nature 2001;**410**:101–105.
38. Kimachi K, Croft M, Grey HM. The minimal number of antigen-major histocompatibility complex class II complexes required for activation of naive and primed T cells. Eur J Immunol 1997;**27**:3310–3317.
39. Irvine DJ, Purbhoo MA, Krogsgaard M, Davis MM. Direct observation of ligand recognition by T cells. Nature 2002;**419**:845–849.
40. Watts TH. T cell activation by preformed, long-lived Ia-peptide complexes. Quantitative aspects. J Immunol 1988;**141**: 3708–3714.
41. Agrawal NG, Linderman JJ. Mathematical modeling of helper T lymphocyte/antigen-presenting cell interactions: analysis of methods for modifying antigen processing and presentation. J Theor Biol 1996;**182**:487–504.
42. Lavoie PM, Dumont AR, McGrath H, Kernaleguen AE, Sekaly RP. Delayed expansion of a restricted T cell repertoire by low-density TCR ligands. Int Immunol 2005;**17**:931–941.
43. von Andrian UH, Mempel TR. Homing and cellular traffic in lymph nodes. Nat Rev Immunol 2003;**3**:867–878.
44. Marchesi VT, Gowans JL. The migration of lymphocytes through the endothelium of venules in lymph nodes: an electron microscope study. Proc R Soc Lond B Biol Sci 1964;**159**:283–290.
45. Girard JP, Springer TA. High endothelial venules (HEVs): specialized endothelium for lymphocyte migration. Immunol Today 1995;**16**:449–457.
46. Davis DM, Dustin ML. What is the importance of the immunological synapse? Trends Immunol 2004;**25**:323–327.
47. Lee KH, et al. The immunological synapse balances T cell receptor signaling and degradation. Science 2003;**302**: 1218–1222.
48. Butcher EC, Picker LJ. Lymphocyte homing and homeostasis. Science 1996;**272**: 60–66.
49. von Andrian UH, Mackay CR. T-cell function and migration. Two sides of the same coin. N Engl J Med 2000;**343**: 1020–1034.
50. Chain B, McCafferty I, Wallace G, Askenase PW. Improvement of the in vitro T cell proliferation assay by a modified method that separates the antigen recognition and IL-2-dependent steps. J Immunol Methods 1987;**99**:221–228.
51. Traynor TR, Herring AC, Dorf ME, Kuziel WA, Toews GB, Huffnagle GB. Differential roles of CC chemokine ligand 2/monocyte chemotactic protein-1 and CCR2 in the development of T1 immunity. J Immunol 2002;**168**:4659–4666.
52. Algood HM, Flynn JL. CCR5-deficient mice control Mycobacterium tuberculosis infection despite increased pulmonary lymphocytic infiltration. J Immunol 2004;**173**:3287–3296.
53. Lazarevic V, Nolt D, Flynn JL. Long-term control of Mycobacterium tuberculosis infection is mediated by dynamic immune responses. J Immunol 2005;**175**: 1107–1117.
54. Lindell DM, Moore TA, McDonald RA, Toews GB, Huffnagle GB. Distinct compartmentalization of CD4+ T-cell effector function versus proliferative capacity during pulmonary cryptococcosis. Am J Pathol 2006;**168**:847–855.
55. Sumen C, Mempel TR, Mazo IB, von Andrian UH. Intravital microscopy: visualizing immunity in context. Immunity 2004;**21**:315–329.
56. Catron DM, Itano AA, Pape KA, Mueller DL, Jenkins MK. Visualizing the first 50 hr of the primary immune response to a soluble antigen. Immunity 2004;**21**: 341–347.
57. Miller MJ, Wei SH, Cahalan MD, Parker I. Autonomous T cell trafficking examined in vivo with intravital two-photon microscopy. Proc Natl Acad Sci USA 2003;**100**: 2604–2609.
58. Meyer-Hermann ME, Maini PK. Interpreting two-photon imaging data of lymphocyte motility. Phys Rev E Stat Nonlin Soft Matter Phys 2005;71:061912.
59. Sprent J, Tough D. T cell death and memory. Science 2001;**293**:245–248.
60. Bajenoff M, et al. Stromal cell networks regulate lymphocyte entry, migration, and territoriality in lymph nodes. Immunity 2006;**25**:989–1001.

61. Castellino F, et al. Chemokines enhance immunity by guiding naive CD8+ T cells to sites of CD4+ T cell-dendritic cell interaction. Nature 2006;**440**:890–895.
62. Okada T, et al. Antigen-engaged B cells undergo chemotaxis toward the T zone and form motile conjugates with helper T cells. PLoS Biol 2005;**3**:el50.
63. Miller MJ, Safrina O, Parker I, Cahalan MD. Imaging the single cell dynamics of CD4+ T cell activation by dendritic cells in lymph nodes. J Exp Med 2004;**200**: 847–856.
64. Miyasaka M, Tanaka T. Lymphocyte trafficking across high endothelial venules: dogmas and enigmas. Nat Rev Immunol 2004;**4**:360–370.
65. Cahill RN, Frost H, Trnka Z. The effects of antigen on the migration of recirculating lymphocytes through single lymph nodes. J Exp Med 1976;**143**:870–888.
66. Gretz JE, Anderson AO, Shaw S. Cords, channels, corridors and conduits: critical architectural elements facilitating cell interactions in the lymph node cortex. Immunol Rev 1997;**156**:11–24.
67. Bajenoff M, Granjeaud S, Guerder S. The strategy of T cell antigen-presenting cell encounter in antigen-draining lymph nodes revealed by imaging of initial T cell activation. J Exp Med 2003;**198**: 715–724.
68. Randolph GJ, Angeli V, Swartz MA. Dendritic-cell trafficking to lymph nodes through lymphatic vessels. Nat Rev Immunol 2005;**5**:617–628.
69. Westermann J, Bode U, Pabst R. Migration of naive and memory T cells in vivo. Immunol Today 1998;**19**:143–144.
70. Rosenberg YJ, Janossy G. The importance of lymphocyte trafficking in regulating blood lymphocyte levels during HIV and SIV infections. Semin Immunol 1999;**11**: 139–154.
71. Miller MJ, Hejazi AS, Wei SH, Cahalan MD, Parker I. T cell repertoire scanning is promoted by dynamic dendritic cell behavior and random T cell motility in the lymph node. Proc Natl Acad Sci USA 2004;**101**:998–1003.
72. Marino S, Kirschner DE. The human immune response to Mycobacterium tuberculosis in lung and lymph node. J Theor Biol 2004;**227**:463–486.
73. Marino S, Pawar S, Fuller CL, Reinhart TA, Flynn JL, Kirschner DE. Dendritic cell trafficking and antigen presentation in the human immune response to Mycobacterium tuberculosis. J Immunol 2004;**173**: 494–506.
74. Sprent J. Circulating T and B lymphocytes of the mouse. I. Migratory properties. Cell Immunol 1973;**7**:10–39.
75. Sprent J, Basten A. Circulating T and B lymphocytes of the mouse. II. Lifespan. Cell Immunol 1973;**7**:40–59.
76. Swain SL, et al. From naive to memory T cells. Immunol Rev 1996;**150**:143–167.
77. Mims CA, Nash A, Stephen J. Mims' Pathogenesis of Infectious Disease, 5th edn. San Diego: Academic Press, 2001.
78. Miller DM, et al. Human cytomegalovirus inhibits major histocompatibility complex class II expression by disruption of the Jak/Stat pathway. J Exp Med 1998;**187**: 675–683.
79. Mahanty S, Hutchinson K, Agarwal S, McRae M, Rollin PE, Pulendran B. Cutting edge: impairment of dendritic cells and adaptive immunity by Ebola and Lassa viruses. J Immunol 2003;**170**:2797–2801.
80. Fenton MJ. Macrophages and tuberculosis. Curr Opin Hematol 1998;**5**:72–78.
81. Moreno C, Mehlert A, Lamb J. The inhibitory effects of mycobacterial lipoarabinomannan and polysaccharides upon polyclonal and monoclonal human T cell proliferation. Clin Exp Immunol 1988;**74**:206–210.
82. Hmama Z, Gabathuler R, Jefferies WA, de Jong G, Reiner NE. Attenuation of HLA-DR expression by mononuclear phagocytes infected with Mycobacterium tuberculosis is related to intracellular sequestration of immature class II heterodimers. J Immunol 1998;**161**:4882–4893.
83. Noss EH, Harding CV, Boom WH. Mycobacterium tuberculosis inhibits MHC class II antigen processing in murine bone marrow macrophages. Cell Immunol 2000;**201**: 63–74.
84. unaids.org. UNAIDS/WHO AIDS Epidemic Update: December 2005. URL http:// www.unaids.org, 2005.
85. Edelstein-Keshet L. Mathematical Models in Biology. New York: Random House, 1988.
86. Murray JD. Mathematical Biology. New York: Springer-Verlag, 1989.
87. Keener JP, Sneyd J. Mathematical Physiology. New York: Springer, 1998.
88. Segel LA, Cohen IR. Design Principles for the Immune System and other Distributed Autonomous Systems. Oxford: Oxford University Press, 2001.
89. Grimm V, Railsback SF. Individual-based Modeling and Ecology. Princeton: Princeton University Press, 2005.
90. Lauffenburger DA, Linderman JL Receptors: Models for Binding, Trafficking and Signaling. New York: Oxford University Press, 1993.
91. Brauer F, Castillo-Châavez C. Mathematical Models in Population Biology and Epidemiology. New York: Springer, 2001.
92. Armitage P, Berry G, Matthews JNS. Statistical Methods in Medical Research, 4th edn. Malden, MA: Blackwell Science, 2001.
93. Lund O. Immunological Bioinformatics. Cambridge, MA: MIT Press, 2005.
94. Ewens WJ, Grant GR. Statis[t]ical Methods in Bioinformatics: An Introduction, 2nd edn. New York: Springer, 2005.
95. DeAngelis DL, Gross LJ. Individual-based Models and Approaches in Ecology: Populations, Communities, and Ecosystems. New York: Chapman & Hall, 1992.
96. Kirschner DE, Gammack D, Ganguli S, Marino S, Segovia-Juarez J. Understanding the immune response in tuberculosis using different mathematical models and biological scales. SIAM J Multiscale Model Sim 2005;**3**:312–345.
97. Waller A, et al. Receptor binding kinetics and cellular responses of six N-formyl peptide agonists in human neutrophils. Biochemistry 2004;**43**:8204–8216.
98. Blower SM, Dowlatabadi H. Sensitivity and uncertainty analysis of complex-models of disease transmission – an HIV model, as an example. Int Stat Rev 1994;**62**: 229–243.
99. Helton JC, Davis FJ. Illustration of sampling-based methods for uncertainty and sensitivity analysis. Risk Anal 2002;**22**: 591–622.
100. Gammack D, Doering CR, Kirschner DE. Macrophage response to Mycobacterium tuberculosis infection. J Math Biol 2004;**48**:218–242.
101. Segovia-Juarez JL, Ganguli S, Kirschner D. Identifying control mechanisms of granuloma formation during M. tuberculosis infection using an agent-based model. J Theor Biol 2004;**231**:357–376.
102. Meng X-l, Rosenthal R, Rubin DB. Comparing correlated correlation coefficients. Psychol Bull 1992;**111**:172–175.
103. Rammensee HG. Chemistry of peptides associated with MHC class I and class II molecules. Curr Opin Immunol 1995; **7**:85–96.
104. Parker KC, Bednarek MA, Coligan JE. Scheme for ranking potential HLA-A2 binding peptides based on independent binding of individual peptide side-chains. J Immunol 1994;**152**:163–175.
105. Murugan N, Dai Y. Prediction of MHC class II binding peptides based on an iterative learning model. Immunome Res 2005;**1**:6.
106. Mallios RR. Class II MHC quantitative binding motifs derived from a large molecular database with a versatile iterative stepwise discriminant analysis meta-algorithm. Bioinformatics 1999;**15**:432–439.
107. Mallios RR. Predicting class II MHC/peptide multi-level binding with an iterative stepwise discriminant analysis meta-algorithm. Bioinformatics 2001;**17**:942–948.

108. Mallios RR. A consensus strategy for combining HLA-DR binding algorithms. Hum Immunol 2003;**64**:852–856.
109. Doytchinova IA, Flower DR. Quantitative approaches to computational vaccinology. Immunol Cell Biol 2002;**80**:270–279.
110. Doytchinova IA, Flower DR. Towards the in silico identification of class II restricted T-cell epitopes: a partial least squares iterative self-consistent algorithm for affinity prediction. Bioinformatics 2003;**19**: 2263–2270.
111. Honeyman MC, Brusic V, Stone NL, Harrison LC. Neural network-based prediction of candidate T-cell epitopes. Nat Biotechnol 1998;**16**:966–969.
112. Milik M, et al. Application of an artificial neural network to predict specific class I MHC binding peptide sequences. Nat Biotechnol 1998;**16**:753–756.
113. Buus S, et al. Sensitive quantitative predictions of peptide-MHC binding by a 'Query by Committee' artificial neural network approach. Tissue Antigens 2003;**62**: 378–384.
114. Noguchi H, et al. Hidden markov model-based prediction of antigenic peptides that interact with MHC class II molecules. J Biosci Bioeng 2002;**94**:264–270.
115. Zhao Y, Pinilla C, Valmori D, Martin R, Simon R. Application of support vector machines for T-cell epitopes prediction. Bioinformatics 2003;**19**:1978–1984.
116. Bhasin M, Raghava GP. Prediction of CTL epitopes using QM, SVM and ANN techniques. Vaccine 2004;**22**: 3195–3204.
117. Altuvia Y, Sette A, Sidney J, Southwood S, Margalit H. A structure-based algorithm to predict potential binding peptides to MHC molecules with hydrophobic binding pockets. Hum Immunol 1997;**58**:1–11.
118. Schueler-Furman O, Altuvia Y, Sette A, Margalit H. Structure-based prediction of binding peptides to MHC class I molecules: application to a broad range of MHC alleles. Protein Sci 2000;**9**:1838–1846.
119. Altuvia Y, Margalit H. A structure-based approach for prediction of MHC-binding peptides. Methods 2004;**34**:454–459.
120. Bui HH, Schiewe AJ, von Grafenstein H, Haworth IS. Structural prediction of peptides binding to MHC class I molecules. Proteins 2006;**63**:43–52.
121. Fagerberg T, Cerottini JC, Michielin O. Structural prediction of peptides bound to MHC class I. J Mol Biol 2006;**356**: 521–546.
122. Yu K, Petrovsky N, Schonbach C, Koh JY, Brusic V. Methods for prediction of peptide binding to MHC molecules: a comparative study. Mol Med 2002;**8**:137–148.
123. Brusic V, Bajic VB, Petrovsky N. Computational methods for prediction of T-cell epitopes – a framework for modelling, testing, and applications. Methods 2004; **34**:436–443.
124. Rammensee H, Bachmann J, Emmerich NP, Bachor OA, Stevanovic S. SYFPEITHI: database for MHC ligands and peptide motifs. Immunogenetics 1999;**50**:213–219.
125. Raghava GP. MHCBench – Evaluation of MHC Binding Peptide Prediction Algorithms. URL http://www.imtech.res.in/raghava/mhcbench
126. Sercarz EE, Maverakis E. Mhc-guided processing: binding of large antigen fragments. Nat Rev Immunol 2003;**3**:621–629.
127. Nielsen M, et al. Improved prediction of MHC class I and class II epitopes using a novel Gibbs sampling approach. Bioinformatics 2004;**20**:1388–1397.
128. Bartnes K, Leon F, Briand JP, Travers PJ, Hannestad K. N-terminal elongation of a peptide determinant beyond the first primary anchor improves binding to H-2 I-Ad and HLA-DR1 by backbone-dependent and aromatic side chain-dependent interactions, respectively. Eur J Immunol 1999;**29**: 189–195.
129. Fleckenstein B, Jung G, Wiesmuller KH. Quantitative analysis of peptide-MHC class II interaction. Semin Immunol 1999; **11**:405–416.
130. Petrovsky N, Brusic V. Virtual models of the HLA class I antigen processing pathway. Methods 2004;**34**:429–435.
131. Donnes P, Kohlbacher O. Integrated modeling of the major events in the MHC class I antigen processing pathway. Protein Sci 2005;**14**:2132–2140.
132. Singer DF, Linderman JJ. The relationship between antigen concentration, antigen internalization, and antigenic complexes: modeling insights into antigen processing and presentation. J Cell Biol 1990;**111**: 55–68.
133. Singer DF, Linderman JJ. Antigen processing and presentation: how can a foreign antigen be recognized in a sea of self proteins? J Theor Biol 1991;**151**:385–404.
134. Chang ST, Linderman JJ, Kirschner DE. Multiple mechanisms allow Mycobacterium tuberculosis to continuously inhibit MHC class II-mediated antigen presentation by macrophages. Proc Natl Acad Sci USA 2005;**102**:4530–4535.
135. Sallusto F, Cella M, Danieli C, Lanzavecchia A. Dendritic cells use macropinocytosis and the mannose receptor to concentrate macromolecules in the major histocompatibility complex class II compartment: downregulation by cytokines and bacterial products. J Exp Med 1995;**182**:389–400.
136. Laupeze B, et al. Differential expression of major histocompatibility complex class Ia, Ib, and II molecules on monocytes-derived dendritic and macrophagic cells. Hum Immunol 1999;**60**:591–597.
137. Segel LA. Modeling Dynamic Phenomena in Molecular and Cellular Biology. Cambridge: Cambridge University Press, 1984.
138. Gammack D, Ganguli S, Marino S, Segovia-Juarez JL, Kirschner D. Understanding granuloma formation using different mathematical and biological scales. SIAM J Multiscale Model Sim 2005;**3**: 312–345.
139. Stoll S, Delon J, Brotz TM, Germain RN. Dynamic imaging of T cell-dendritic cell interactions in lymph nodes. Science 2002;**296**:1873–1876.
140. Jacquez JA. Compartmental Analysis in Biology and Medicine, 3rd edn. Ann Arbor: BioMedware, 1996.
141. Bajaria SH, Webb G, Cloyd M, Kirschner D. Dynamics of naive and memory CD4+ T lymphocytes in HIV-1 disease progression. J Acquir Immune Defic Syndr 2002;**30**: 41–58.
142. Ye P, Kourtis A, Kirschner D. The effects of different HIV type 1 strains of human thymic function. AIDS Res Hum Retroviruses 2002;**18**:1239–1251.
143. Bajaria SH, Kirschner DE. CTL action during HIV-1. In: Tan W-Y, Wu H, eds. Deterministic and Stochastic Models for AIDS Epidemics and HIV Infection with Intervention. Hackensack, NJ: World Scientific Publisher, 2005:219–254.
144. Haase AT. Population biology of HIV-1 infection: viral and CD4+ T cell demographics and dynamics in lymphatic tissues. Annu Rev Immunol 1999;**17**:625–656.
145. Rosenberg Y, Anderson A, Pabst R. HIV-induced decline in blood CD4/CD8 ratios: viral killing or altered lymphocyte trafficking? Immunol Today 1998;**19**:10–16.
146. Barron M, Blyveis N, Palmer B, MaWhinney S, Wilson C. Influence of plasma viremia on defects in number and immunophenotype of blood dendritic cell subsets in human immunodeficiency virus 1-infected individuals. J Infect Dis 2003;**187**:26–37.
147. Wigginton JE, Kirschner D. A model to predict cell-mediated immune regulatory mechanisms during human infection with Mycobacterium tuberculosis. J Immunol 2001;**166**:1951–1967.
148. Holt PG, Schon-Hegrad MA. Localization of T cells, macrophages and dendritic cells in rat respiratory tract tissue: implications for immune function studies. Immunology 1987;**62**:349–356.
149. Stone KC, Mercer RR, Gehr P, Stockstill B, Crapo JD. Allometric relationships of cell numbers and size in the mammalian lung. Am J Respir Cell Mol Biol 1992;**6**: 235–243.

150. Antony VB, et al. Recruitment of inflammatory cells to the pleural space. Chemotactic cytokines, IL-8, and monocyte chemotactic peptide-1 in human pleural fluids. J Immunol 1993;**151**:7216–7223.
151. Mercer RR, Russell ML, Roggli VL, Crapo JD. Cell number and distribution in human and rat airways. Am J Respir Cell Mol Biol 1994;**10**:613–624.
152. Law K, Weiden M, Harkin T, Tchou-Wong K, Chi C, Rom WN. Increased release of interleukin-1 beta, interleukin-6, and tumor necrosis factor-alpha by bronchoalveolar cells lavaged from involved sites in pulmonary tuberculosis. Am J Respir Crit Care Med 1996;**153**:799–804.
153. Condos R, Rom WN, Liu YM, Schluger NW. Local immune responses correlate with presentation and outcome in tuberculosis. Am J Respir Crit Care Med 1998;**157**: 729–735.
154. Young AJ, Hay J. Lymphocyte migration in development and disease. Semin Immunol 1999;**11**:71.
155. Young AJ. The physiology of lymphocyte migration through the single lymph node in vivo. Semin Immunol 1999;**11**:73–83.
156. Holt PG. Antigen presentation in the lung. Am J Respir Crit Care Med 2000;**162**: 151–156.
157. Kepler TB, Perelson AS. Drug concentration heterogeneity facilitates the evolution of drug resistance. Proc Natl Acad Sci USA 1998;**95**:11514–11519.
158. Kirschner D, Webb GF, Cloyd M. Model of HIV-1 disease progression based on virus-induced lymph node homing and homing-induced apoptosis of CD4+ lymphocytes. J Acquir Immune Defic Syndr 2000;**24**: 352–362.
159. Snedecor SJ. Comparison of three kinetic models of HIV-1 infection: implications for optimization of treatment. J Theor Biol 2003;**221**:519–541.
160. Ogg G, et al. Quantitation of HIV-1-specific cytotoxic T lymphocytes and plasma load of viral RNA. Science 1998;**279**:2103–2106.
161. Scott-Algara D, et al. Frequency and phenotyping of human immunodeficiency virus (HIV)-specific CD8+ T cells in HIV-infected children, using major histocompatibility complex class I peptide tetramers. J Infect Dis 2001;**183**:1565–1573.
162. Vlachos DG. A review of multiscale analysis: examples from systems biology, materials engineering, and other fluid-surface interacting systems. Adv Chem Eng 2005;**30**:30–31.
163. Kirschner D. The multi-scale immune response to pathogens: M. tuberculosis as an example. In: Flower D, Timmis J, eds. In silico Immunology. New York: Springer, 2007.
164. Coveney PV, Fowler PW. Modelling biological complexity: a physical scientist's perspective. J R Soc Interface 2005:267–280.
165. Garny A, Noble D, Kohl P. Dimensionality in cardiac modelling. Prog Biophys Mol Biol 2005;**87**:47–66.
166. Pai RK, Convery M, Hamilton TA, Boom WH, Harding CV. Inhibition of IFN-gamma-induced class II transactivator expression by a 19-kDa lipoprotein from Mycobacterium tuberculosis: a potential mechanism for immune evasion. J Immunol 2003;**171**:175–184.
167. Gehring AJ, Rojas RE, Canaday DH, Lakey DL, Harding CV, Boom WH. The Mycobacterium tuberculosis 19-kilodalton lipoprotein inhibits gamma interferon-regulated HLA-DR and Fc gamma R1 on human macrophages through Toll-like receptor 2. Infect Immun 2003;**71**:4487–4497.
168. Fulton SA, et al. Inhibition of major histocompatibility complex II expression and antigen processing in murine alveolar macrophages by Mycobacterium bovis BCG and the 19-kilodalton mycobacterial lipoprotein. Infect Immun 2004;**72**: 2101–2110.
169. Pai RK, Pennini ME, Tobian AA, Canaday DH, Boom WH, Harding CV. Prolonged toll-like receptor signaling by Mycobacterium tuberculosis and its 19-kilodalton lipoprotein inhibits gamma interferon-induced regulation of selected genes in macrophages. Infect Immun 2004;**72**: 6603–6614.
170. FDA. Critical Path Initiative. URL http://www.fda.gov/oc/initiatives/criticalpath
171. Donnes P, Elofsson A. Prediction of MHC class I binding peptides, using SVMHC. BMC Bioinformatics 2002;**3**:25.
172. Hattotuwagama CK, Guan P, Doytchinova IA, Zygouri C, Flower DR. Quantitative online prediction of peptide binding to the major histocompatibility complex. J Mol Graph Model 2004;**22**:195–207.
173. Hobohm U, Scharf M, Schneider R, Sander C. Selection of representative protein data sets. Protein Sci 1992;**1**:409–417.
174. Mika S, Rost B. UniqueProt: creating representative protein sequence sets. Nucleic Acids Res 2003;**31**:3789–3791.
175. Peng G. Mathematical Modeling, Simulation and Analysis Program Area. URL http://www.nibib.nih.gov/publicPage.cfm?pageid = 1228
176. Finney A, Hucka M. Systems biology markup language: level 2 and beyond. Biochem Soc Trans 2003;**31**:1472–1473.
177. Lloyd CM, Halstead MD, Nielsen PF. CellML: its future, present and past. Prog Biophys Mol Biol 2004;**85**:433–450.
178. Webb K, White T. UML as a cell and biochemistry modeling language. Biosystems 2005;**80**:283–302.
179. Pai RK, Askew D, Boom WH, Harding CV. Regulation of class II MHC expression in APCs: roles of types I, III, and IV class II transactivator. J Immunol 2002;**169**: 1326–1333.
180. Chang ST, Ghosh D, Kirschner DE, Linderman JJ. Peptide length-based prediction of peptide-MHC class II binding. Bioinformatics 2006;**22**:2761–2767.